Generic phase portrait analysis of finite-time singularities and generalized Teleparallel gravity *

W. El Hanafy[1,3;1)] G.G.L. Nashed[1,2,3;2)]

[1] Centre for Theoretical Physics, The British University in Egypt, P.O. Box 43, El Sherouk City, Cairo 11837, Egypt
[2] Mathematics Department, Faculty of Science, Ain Shams University, Cairo 11566, Egypt
[3] Egyptian Relativity Group (ERG), Cairo University, Giza 12613, Egypt

Abstract: We analyze the four common types of finite-time singularity using a generic framework of the phase portrait geometric approach. This technique requires the Friedmann system to be written as a one-dimensional autonomous system. We employ a scale factor that has been used widely in the literature to realize the four finite-time singularity types, then we give a detailed discussion for each case showing possible novel models. Moreover, we show how different singularity types can play essential roles in different cosmological scenarios. Among several modified gravity theories, we show that the $f(T)$ cosmology is compatible with the phase portrait analysis, since the field equations include Hubble derivatives only up to first order. Therefore, we reconstruct the $f(T)$ theory which generates these phase portraits. We also perform a complementary analysis using the effective equation of state. Furthermore, we investigate the role of the torsion fluid in realizing the cosmic singularities.

Keywords: inflation, bounce, big brake, ΛCDM, teleparallel gravity

PACS: 04.20.Cv, 04.20.Dw, 04.20.Ex **DOI:** 10.1088/1674-1137/41/12/125103

1 Introduction

The cosmological singularity problem has received attention for a long time. However, many studies have considered only the crashing type, e.g. big bang and big crunch singularities. Recently, after observations of Type Ia supernovae (SNIa), other softer types of singularity have been introduced to the game. Several attempts have been made to investigate the role of quantum effects in smoothing out the singularity [1–3], or to study geodesic completeness and the possibility of crossing the singularity [4–7]. Also, some studies have investigated the effect of the singularity on the cosmic observable quantities [8–10]. On the other hand, nonsingular bounce cosmology could provide an alternative approach to explain cosmic observations. In this scenario, the universe begins with a contraction phase, then it reaches a nonzero minimal length before expansion, and therefore it does not suffer from the trans-Planckian problems of the inflation models [11, 12]. The bouncing universe has gained attention in recent literature, where the cosmic evolution shows interesting features on both the background and the perturbative levels [13–19]. In classical general relativity, one should introduce some fluid with an exotic equation of state to establish these models. However, we find that modified gravity theories could provide an alternative by modifying the gravitational sector. Indeed, modified gravity has been used to successfully describe a bouncing universe, and helps to resolve several problems of these models, e.g. anisotropy and ghost instability problems, c.f. Refs. [20–24]. Also, it is worth analyzing various singularities within the modified gravity framework, which is the target of this paper.

For reasonable cosmological requirements, the universe is usually taken to be homogeneous and isotropic. Thus, we take the metric to be of the Friedmann-Lemaitre-Robertson-Walker (FLRW) form,

$$\mathrm{d}s^2=c^2\mathrm{d}t^2-a(t)^2\delta_{ij}\mathrm{d}x^i\mathrm{d}x^j, \tag{1}$$

where c is the speed of light in vacuum and $a(t)$ is the scale factor of the universe. In modified theories of gravity, one can write the Friedmann system as

$$\rho_{\rm eff}\equiv\frac{3}{\kappa^2}H^2,\quad p_{\rm eff}\equiv-\frac{1}{\kappa^2}\left(2\dot{H}+3H^2\right), \tag{2}$$

where $H\equiv\frac{\dot{a}}{a}$ is the Hubble parameter, the dot denotes the derivative with respect to the cosmic time t, the coupling constant $\kappa^2\equiv8\pi G$, and G is the gravitational constant. We use natural units, i.e. $k_B=c=\hbar=1$. In this case, we can write $\kappa=1/M_p$, where $M_p=2.4\times10^{18}$ GeV is

Received 16 August 2017
∗ Supported by the Egyptian Ministry of Scientific Research (24-2-12)
1) E-mail: waleed.elhanafy@bue.edu.eg
2) E-mail: nashed@bue.edu.eg

the reduced Planck mass. We also denote the effective (total) energy density and the pressure as $\rho_{\rm eff}$ and $p_{\rm eff}$, respectively. We further assume that the effective fluid has a barotropic equation of state, then we can classify the finite-time singularities as in Refs. [25, 26]. In brief, we illustrate the fundamental characteristics of this classification as below. Let the time of the singularity be t_s.

(1) Type I: At $t\to t_s$, the scale factor a, the effective energy density $\rho_{\rm eff}$ and the pressure $p_{\rm eff}$ diverge, i.e. $a\to\infty$, $\rho_{\rm eff}\to\infty$, and $|p_{\rm eff}|\to\infty$. A Type I singularity is of crushing type and known as a "*big rip*" singularity, c.f. [25].

(2) Type II: At $t\to t_s$, the scale factor a and the effective energy density $\rho_{\rm eff}$ approach finite values, while the effective pressure diverges, i.e. $a\to a_s$, $\rho_{\rm eff}\to\rho_s$ and $|p_{\rm eff}|\to\infty$. A Type II singularity is not of a crushing type and is known as "*sudden*" singularity, c.f. [1, 4, 10, 27, 28].

(3) Type III : At $t\to t_s$, only the scale factor tends to a finite value, while the effective energy density and the pressure both diverge, i.e. $a\to a_s$, $\rho_{\rm eff}\to\infty$ and $|p_{\rm eff}|\to\infty$. Type III is of the crushing type.

(4) Type IV : At $t\to t_s$, all three quantities mentioned approach finite values, i.e. $a\to a_s$, $\rho_{\rm eff}\to\rho_s$ and $|p_{\rm eff}|\to p_s$. In addition, the Hubble parameter and its first derivative are finite, while its second/higher derivatives diverge. A Type IV singularity is the softest (not of the crushing type) of the four types, c.f. Refs. [10, 22, 25, 29–31].

This work is devoted to analyzing the finite-time singularity types using a generic framework of the phase portrait geometric approach. This technique assumes the Friedmann system to be written as a "*one dimensional autonomous system*" [32, 33]. We organize the paper as follows. In Section 2, we review the phase portrait analysis and its application in cosmology. We also describe a scale factor that can realize the four singularity types, then we give a detailed discussion for each case. Moreover, we show how different singularity types can play essential roles in different cosmological scenarios. In Section 3, we show that the $f(T)$ gravity among several modified gravity theories is compatible with the phase portrait technique. We also reconstruct the $f(T)$ theory which generates these phase portraits. In Section 4, we perform a complementary analysis using the effective equation of state. Furthermore, we investigate the role of the torsion fluid in realizing the cosmic singularities. In Section 5, we summarize the work.

2 Phase portraits of finite-time singularities

In Eq. (2), we define the effective density energy and the effective pressure as $\rho_{\rm eff}=\sum_i\rho_i$ and $p_{\rm eff}=\sum_i p_i$ respectively. The index i denotes the fluid component. In this case, if we consider the effective matter to have a linear equation of state, we define the effective equation of state parameter as

$$\omega_{\rm eff}\equiv\frac{p_{\rm eff}}{\rho_{\rm eff}}=-1-\frac{2}{3}\frac{\dot{H}}{H^2}. \tag{3}$$

In fact, the differential equation represents a one-dimensional autonomous system, if we can write $\dot{H}\equiv\mathcal{F}(H)$. The proper way to fulfill this condition is to have a fixed effective equation of state parameter which reproduces general relativity as a special case, or to have a dynamical effective equation of state but as a function of H only. We are interested in the more general case, $\omega_{\rm eff}\equiv\omega_{\rm eff}(H)$, so we rewrite Eq. (3) as

$$\dot{H}=-\frac{3}{2}(1+\omega_{\rm eff}(H))H^2\equiv\mathcal{F}(H). \tag{4}$$

As a consequence, we can always interpret this differential equation as a vector field on a line introducing one of the basic techniques of dynamics. This view, geometrically, is by drawing $\dot{H}$ versus H, which helps to analyze the cosmic model in a clear and transparent way even without solving the system. In order to fix our notations, we follow Ref. [34] in calling Eq. (4) the *phase portrait*, while its solution $H(t)$ is the *phase trajectory*. Thus, the phase portrait corresponds to any theory can be drawn in an $(\dot{H}-H)$ *phase-space* of Friedmann's system. In this space each point is a *phase point* and could serve as an initial condition.

For C^∞ monotonic phase portraits, it has been shown that the fixed points ($\dot{H}=0$) cannot be reached in a finite time [32]. In fact, the fixed point, in addition, would be Minkowskian, if $H=0$ and $\dot{H}=0$. Otherwise, it would be de Sitter, i.e. $H\neq0$ and $\dot{H}=0$. For a phase portrait (4), if the universe begins at a fixed point, it will stay forever at that point. The stability classification of a fixed point can be performed by allowing a small perturbation about it, and investigating whether the perturbation decays or grows. Generally, if the slope of the phase portrait is positive at the fixed point, the perturbation grows and the fixed point in this case is unstable (repeller or source). If the slope is negative, the fixed point is stable (attractor or sink). However, if the slope alters its sign at the fixed point, it is semi-stable and the solution is stable from one side and unstable from the other side. For an infinite slope case (e.g. cusps) there are infinitely many solutions starting from the same initial condition so that the phase point doesn't know how to move. In this case the geometric approach collapses.

We summarize phase portrait analysis as a useful tool to qualitatively describe the dynamical behavior of a flat FLRW model by constructing its ($\dot{H}$-H) phase space diagram [32]. When the system is autonomous and one-dimensional, the dynamics are controlled by the asymp-

totic behavior of the phase portrait and by its fixed points. In general, after identifying the fixed points, we next define the zero acceleration curve by setting the deceleration parameter $q\equiv-\frac{a\ddot{a}}{\dot{a}^2}=0$, i.e., $\dot{H}=-H^2$, which splits the phase space into two regions. The inner region characterizes the decelerated phases. This is shown by the shaded region in Fig. 1. However, the unshaded region represents the accelerated phases. We classify the different phases in Fig. 1 as follows:

(1) Region I: an accelerated contracting universe as $q<0$ and $H<0$.

(2) Region II: a decelerated contacting universe as $q>0$ and $H<0$.

(3) Region III: a decelerated expanding universe as $q>0$ and $H>0$, which characterizes the usual FLRW models.

(4) Region IV: an accelerated expanding universe as $q<0$ and $H>0$, which characterizes the so-called inflation or dark energy phases.

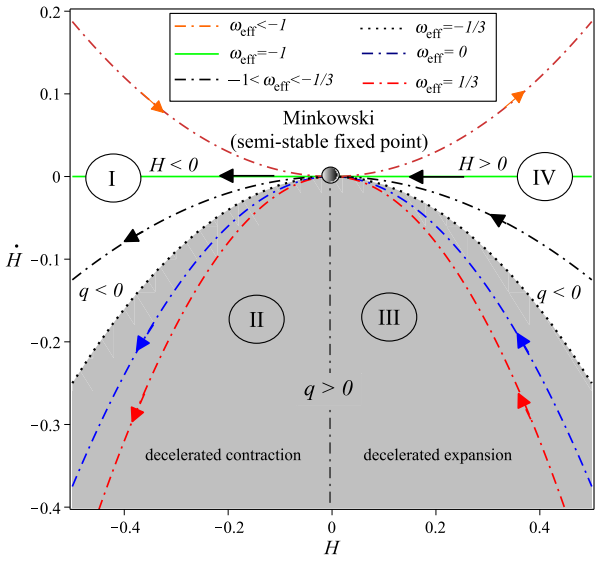

Fig. 1. (color online) Phase portraits 4 corresponding to different values of the effective equation of state parameters. The origin of the phase space is Minkowski space, and the zero acceleration curve ($\omega_{\rm eff}=-1/3$) splits the space into deceleration (shaded) and acceleration (unshaded) regions, while the negative (positive) Hubble regions are contraction (expansion) regions. This subdivides the phase space into four regions. We denote them as regions I–IV.

We consider the following scale factor in order to realize the four singularity types [29, 35]:

$$a(t)=\mathrm{e}^{f_0(t-t_s)^{2(1+\varepsilon)}}. \tag{5}$$

Introducing the new parameters $\alpha\equiv1+2\varepsilon$ and $\beta\equiv2(1+\varepsilon)f_0=(1+\alpha)f_0$, we write the Hubble parameter as

$$H(t)=\beta(t-t_s)^{\alpha}, \tag{6}$$

where α is dimensionless and β has a dimension of $[\text{time}]^{-1-\alpha}$. We note that in the Planck unit system, the Hubble parameter is measured in GeV and time is measured in $[\text{GeV}]^{-1}$, so β is measured in $[\text{GeV}]^{1+\alpha}$. The classification of finite-time singularities can be realized by the scale factor (5). According to different choices of the parameter α, as given in Table 1, the four types of singularities could occur at $t=t_s$.

Table 1. Singularity types classification according to the choice of the α parameter in Eq. (5).

$t\to t_s$	Type I ($\alpha<-1$)	Type II ($0<\alpha<1$)	Type III ($-1<\alpha<0$)	Type IV* ($\alpha>1$)
$a\to a_s$	×	✓	✓	✓
$H\to H_s$	×	✓	×	✓
$\dot{H}\to\dot{H}_s$	×	×	×	✓
$\rho_{\rm eff}\to\rho_s$	×	✓	×	✓
$\lvert p_{\rm eff}\rvert\to p_s$	×	×	×	✓

*The higher derivatives $\mathrm{d}^nH/\mathrm{d}t^n$ diverge, $n\geqslant2$.

Using the inverse relation of Eq. (6), we express the time in terms of the Hubble parameter,

$$t(H)=t_s+\left(\frac{H}{\beta}\right)^{\frac{1}{\alpha}}. \tag{7}$$

Thus, we write the implicit differentiation $\dot{H}\equiv\dot{H}(H)$ as

$$\dot{H}=\alpha H\left(\frac{H}{\beta}\right)^{-\frac{1}{\alpha}}. \tag{8}$$

The above relation represents a one-dimensional autonomous system, whereas its graphical representation provides the *phase portrait* of the cosmic evolution, which can be seen clearly in the $\left(H\text{-}\dot{H}\right)$ phase space for different choices of the parameter α.

In general, the phase portrait (8) evolves towards a fixed point at which $\dot{H}=0$, or a point at which $\dot{H}\to\pm\infty$. The former can be achieved at $H=0$ where $\alpha<0$ or $\alpha>1$, so we expect the phase portraits associated with Type I, III and IV singularities to pass through a Minkowskian fixed point $\left(H=0,\ \dot{H}=0\right)$. The latter does not always mean that the system is singular at $\dot{H}\to\pm\infty$. It has been shown that if the asymptotic behavior of $\dot{H}$ grows linearly or slower, the solution will not have a finite-time singularity [32]. This can be shown, since the singularity time

$$t_s=\int_{H_0}^{\pm\infty}\frac{\mathrm{d}H}{\dot{H}}. \tag{9}$$

Using Eq. (8), it is clear that the phase portrait belongs to the power-law family, i.e. $\dot{H}\propto H^{\gamma}$. It is not difficult

to realize that the big bang (singular) model is a special case where $\gamma=2$. In general, the time to reach the singularity is finite

$$t_s=\frac{1}{(\gamma-1)H_0^{\gamma-1}};\quad \text{if } \gamma>1.$$

On the other hand, the time to reach the singularity could be infinite

$$t_s\to\pm\infty;\quad \text{if } \gamma\leqslant 1.$$

Therefore, the phase portrait (8) evolves towards $\dot{H}\to\pm\infty$ in an infinite time where $\alpha>0$, and we expect that the phase portraits associated with Type II and IV singularities only to be free from singularities of crashing type at $H\to\pm\infty$.

2.1 Type I singularity phase portrait

This singularity occurs when the cosmic time approaches $t\to t_s$. The scale factor a, the effective energy density $\rho_{\rm eff}$ and the pressure $p_{\rm eff}$ diverge, i.e. $a\to\infty$, $\rho_{\rm eff}\to\infty$, and $|p_{\rm eff}|\to\infty$. A Type I singularity is of crushing type and is known as a "*big rip*" singularity, c.f. Ref. [25]. Using the scale factor (5), the Type I singularity case occurs when $\alpha<-1$. In this case, we have $\beta=f_0(1+\alpha)<0$, when $f_0>0$ and $\beta=f_0(1+\alpha)>0$, when $f_0<0$. Different cases of the phase portraits corresponding to Eq. (8) are given in Fig. 2. In general, one-dimensional autonomous systems are dominated by fixed points, while the time required to reach any of these points is infinite. In other words, the fixed points split the phase space into separate regions. This can be easily seen in Friedmann cosmology, since the time is given as

$$t=\int_{H_0}^{H_f}\frac{{\rm d}H}{\dot{H}}\to\pm\infty. \tag{10}$$

At a fixed point H_f, we have $\dot{H}=0$, and the time required to reach it is infinite. The phase portraits in Fig. 2 show two possible cosmic behaviors according to the choice of $f_0>0$ ($f_0<0$), and consequently $\beta<0$ ($\beta>0$). We discuss both cases as follows.

2.1.1 $f_0>0$ ($\beta<0$)

The corresponding phase portrait is given in Fig. 2(a). The universe is allowed only in the phantom regime. It begins with a big rip singularity at

$$t_s=\int_{-\infty}^{H_0}\frac{{\rm d}H}{\dot{H}}=\left|\frac{H_0}{\beta}\right|^{1/\alpha},$$

from a particular value $H_0<0$. Since the universe evolves in $\dot{H}>0$ and $H<0$ phase space with a Minkowskian fixed point fate, the universe experiences an eternal accelerating contraction.

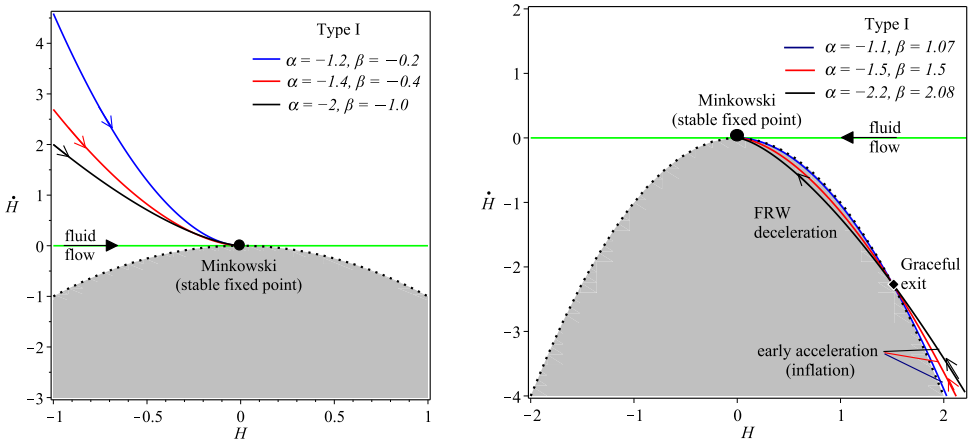

(a) $f_0>0(\beta<0)$ (b) $f_0<0(\beta>0)$

Fig. 2. (color online) Phase portraits of finite-time singularities of Type I for different choices of the parameter $\alpha<-1$ in Eqs. (8).

2.1.2 $f_0<0$ ($\beta>0$)

The corresponding phase portrait is given in Fig. 2**??**. The universe evolves in a non-phantom regime. It begins with a big bang at $t_s=(H_0/\beta)^{1/\alpha}$ from a present Hubble value $H_0>0$. Interestingly, for suitable values of the parameters α and β, the phase portrait provides a graceful exit inflationary model. The universe could begin with an early accelerated expansion phase (inflation), however, it could be followed by a decelerated expansion phase (FLRW). At the graceful exit transition, the phase portrait should cut the zero acceleration curve ($\dot{H}=-H^2$) from acceleration to deceleration. Using Eq. (8), at the transition $H_{\rm inf}$, the two parameters can be related by

$$\beta=H_{\rm inf}\left(-\frac{H_{\rm inf}}{\alpha}\right)^{\alpha}. \tag{11}$$

For any value of $\alpha<-1$, the above equation can predict the value of β when the Hubble parameter at the end of inflation $H_{\rm inf}$ is known. For more detailed discussion about the possible values of α and β to realize a graceful exit inflation, see Section 2.5.

2.1.3 Physical description

In conclusion, we find that the case of $\beta>0$ is more interesting than the other cases, since it provides a graceful exit inflation model. In Section 2.5, we will obtain suitable values of the parameters α and β which realize inflation at a suitable energy scale.

2.2 Type II singularity phase portrait

This singularity occurs when the cosmic time approaches $t\to t_s$. The scale factor a and the effective energy density $\rho_{\rm eff}$ approach finite values, while the effective pressure diverges, i.e. $a\to a_s$, $\rho_{\rm eff}\to\rho_s$ and $|p_{\rm eff}|\to\infty$. A Type II singularity is not of a crushing type and is known as a "*sudden*" singularity, c.f. Refs. [1, 4, 10, 27, 28]. Using the scale factor (5), the Type II singularity case occurs when $0<\alpha<1$. In this case, we have $\beta=f_0(1+\alpha)<0$, when $f_0<0$, while $\beta=f_0(1+\alpha)>0$, when $f_0>0$. Different cases of the phase portraits corresponding to Eq. (8) are given in Fig. 3. It is clear that the finite-time singularity of type II is not a fixed point, but it occurs, commonly, when $\dot H$ diverges as $H\to H_s=0$. However, we split the discussion of the phase portraits corresponding to the Type II singularity into two main categories according to the choice of $f_0<0$ and $f_0>0$ in the given range $0<\alpha<1$ as follows.

2.2.1 $f_0<0$ ($\beta<0$)

In this category, three patterns can be obtained, depending on the value of α. Therefore, we have the following subclasses.

Case 1. $\alpha=\frac{1}{n}$ ($n>1$ is an odd positive integer): The corresponding phase portraits are indicated by the dashed curves in Fig. 3(a). In the positive H region, the fluid evolves towards the left (decreasing H), approaching a future sudden singularity $H_s=0$, where the time to reach it is finite.

$$t_s=\int_{H_0}^{H_s=0}\frac{{\rm d}H}{\dot H}=-\left(\frac{H_0}{\beta}\right)^{1/\alpha},$$

where $H_0>0$ denotes the present Hubble value. In the negative H region, the cosmic fluid evolves towards rge left (decreasing H). It begins with a sudden singularity $\dot H\to-\infty$ at $H_s=0$, then it goes into a decelerated contraction phase. After that it enters an accelerated contraction phase with a de Sitter fate as $H\to-\infty$. Similar models have been studied in detail in Ref. [4].

Case 2. $\alpha=\frac{1}{n}$ ($n>1$ is an even positive integer): The corresponding phase portraits are given in Fig. 3(b). Notably, in this subclass, the phase portraits corresponding to $\pm\beta$ are identical. In the negative H region, the cosmic fluid flows towards the left (decreasing H). However, in the positive H region, the fluid flows towards the right (increasing H). So we may consider these two regions as separate regions. The left-hand region ($H<0$) begins with a finite-time singularity of type II, where the universe evolves from a decelerated contraction to an accelerated expansion towards a de Sitter space. The right-hand region ($H>0$) shows that the universe has an initial finite-time singularity of type II, but evolves effectively towards a de Sitter space in a phantom regime.

Case 3. $\alpha=\frac{a}{b}$ ($a<b$ and $\frac{a}{b}\neq\frac{1}{n}$): The corresponding phase portraits are indicated by the dashed curves in Fig. 3(c), which shows that the positive H region is not valid for these values of α. However, the dynamical behavior of the universe is the same as in cases 1 and 2 above, in the $H<0$ region.

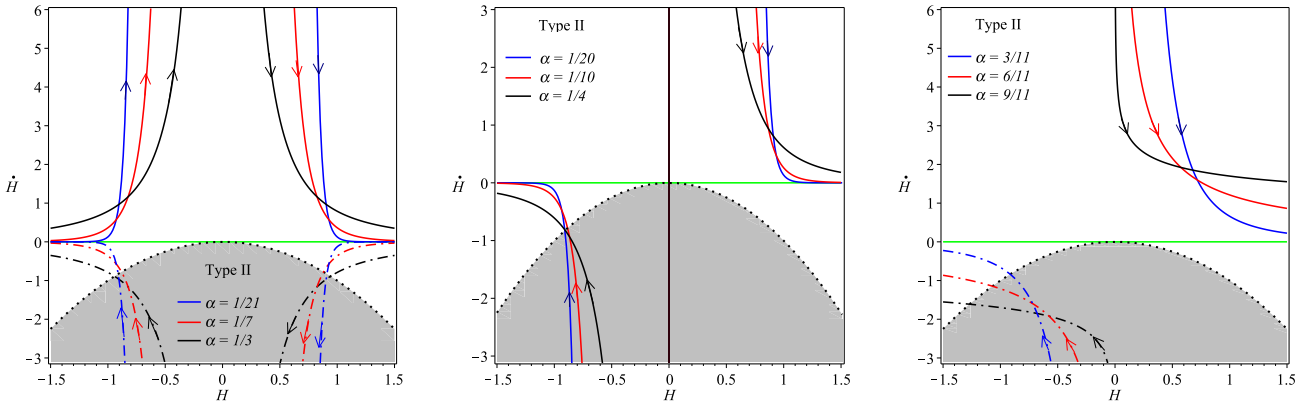

(a) $\alpha=\frac{1}{n}$, n = odd (b) $\frac{1}{n}$, n = even (c) $\alpha=\frac{a}{b}$, $a<b$ and $\frac{a}{b}\neq\frac{1}{n}$

Fig. 3. (color online) Phase portraits of finite-time singularities of Type II for different choices of the parameter $0<\alpha<1$ in Eq. (8). The dashed curves correspond to $f_0<0$ ($\beta<0$), and the solid curves correspond to $f_0>0$ ($\beta>0$). Same-color curves show the same value of α. The phase portraits of (b) are typical for both $\beta<0$ and $\beta>0$.

2.2.2 $f_0>0$ ($\beta>0$)

In this category, similarly, three patterns can be obtained depending on the value of α. Therefore, we have the following subclasses.

Case 1. $\alpha=\frac{1}{n}$ ($n>1$ is an odd positive integer): The corresponding phase portraits are indicated by the solid curves in Fig. 3(a). In the negative H region (contraction phase), the cosmic fluid flows towards the right (increasing H). For a given value $H_0<0$, the universe has no initial singularity as

$$t=\int_{-\infty}^{H_0}\frac{\mathrm{d}H}{\dot{H}}=-\infty.$$

However, the time required to reach the singular phase is

$$t_s=\int_{H_0}^{0}\frac{\mathrm{d}H}{\dot{H}}=-\left|\frac{H_0}{\beta}\right|^{1/\alpha}.$$

In the positive H region (expansion phase), the fluid also flows to the right. The time from the singular phase $H=0$ to a given phase $H_0>0$ is $t_s=\left(\frac{H_0}{\beta}\right)^{1/\alpha}$, while the universe has no future singularity as the time to reach $H\to\infty$ is infinite. Since $\dot{H}>0$ in both regions, $H<0$ and $H>0$, and time is extended as $-\infty<t<\infty$. This case gives rise to a bouncing model with a singularity of type II at the bouncing point $H=0$. In this case, we can restrict the Hubble length to a minimal value of the Planck length and use junction conditions to cross the singularity, providing a soft rebirth of the expanding universe after the contraction phase [4].

Case 2. $\alpha=\frac{1}{n}$ ($n>1$ is an even positive integer): The corresponding phase portraits are given in Fig. 3(b). As mentioned in Section 2.2.1, the phase portraits of $\pm\ \beta$ are identical. Therefore, we expect the same description as given before.

Case 3. $\alpha=\frac{a}{b}$ ($a<b$ and $\frac{a}{b}\neq\frac{1}{n}$): The corresponding phase portraits are indicated by the solid curves in Fig. 3(c), which shows that the negative H region is not valid for these values of α. However, the dynamical behavior of the universe is the same as in cases 1 and 2 above, in the $H>0$ region.

2.2.3 Physical description

In conclusion, a finite-time singularity of type II could act as an attractor or repeller depending on the choice of the model parameter in the given range $0<\alpha<1$. Remarkably, case 1, for $\beta>0$ values, provides a big bounce cosmology in the phantom regime, where the bouncing point coincides with a sudden singularity. Also, case 1, for $\beta<0$ values, provides a big brake cosmology, which has been shown to be compatible with the SNIa data [4]. In both cases, the first derivative of the scale factor is finite, so the Christoffel symbols are regular and the geodesics are well behaved, and thus the singularity becomes traversable. In addition to the kinematic description of the phase portrait method, a complementary investigation using torsion gravity is available in Section 4.2.

2.3 Type III singularity phase portrait

This singularity occurs when the cosmic time approaches $t\to t_s$. Only the scale factor tends to a finite value, while the effective energy density and the pressure both diverge, i.e. $a\to a_s$, $\rho_{\rm eff}\to\infty$ and $|p_{\rm eff}|\to\infty$. Type III is of the crushing type. Using the scale factor (5), the Type III singularity case occurs when $-1<\alpha<0$. In this case, we have $\beta=f_0(1+\alpha)<0$, when $f_0<0$, while $\beta=f_0(1+\alpha)>0$, when $f_0>0$. Different cases of the phase portraits corresponding to Eq. (8) are given in Fig. 4. Remarkably, the transition from deceleration to acceleration, in the $H>0$ region, can be realized for $-1<\alpha<0$. Since the evolution pattern is sensitive to the choices of α and β, we discuss different cases as follows.

2.3.1 $f_0<0$ ($\beta<0$)

In this category, three patterns can be obtained, depending on the value of α. Therefore, we have the following subclasses.

Case 1. $\alpha=-\frac{1}{n}$ ($n>1$ is an odd positive integer): The phase portraits for some particular choices of α are indicated by the dashed curves in Fig. 4(a), where the Minkowskian fixed point at the origin of the phase space is a common point for all portraits. Minkowski space, in this case, is a semi-stable fixed point. Since the universe requires an infinite time to reach this Minkowskian space, we find that $H<0$ and $H>0$ are two separate regions. Firstly, we discuss the $H<0$ region, where the universe begins with an initial finite-time singularity of Type III as H and $\dot{H}$ diverge at $t\to t_s$, where

$$t_s=\int_{H_0<0}^{-\infty}\frac{\mathrm{d}H}{\dot{H}}=\left(\frac{H_0}{\beta}\right)^{1/\alpha},$$

from some value $H_0<0$. Then, it evolves in the increasing H direction towards a future fixed point $H=0$. However, the time requires to approach that point is infinite, so the universe has no future finite-time singularity. Secondly, in the $H>0$ region, the universe has no initial singularity, since the time to reach its Minkowskian origin is infinite. However, the universe evolves in a phantom regime towards a future finite-time singularity of Type III as $t\to t_s$, where

$$t_s=\int_{H_0>0}^{\infty}\frac{\mathrm{d}H}{\dot{H}}=\left(\frac{H_0}{\beta}\right)^{1/\alpha},$$

from some value $H_0>0$.

Case 2. $\alpha=-\frac{1}{n}$ ($n>1$ is an even positive integer): The corresponding phase portraits are indicated by the dashed curves in Fig. 4(b). Notably, in this subclass, the phase portraits corresponding to $\pm\ \beta$ are identical.

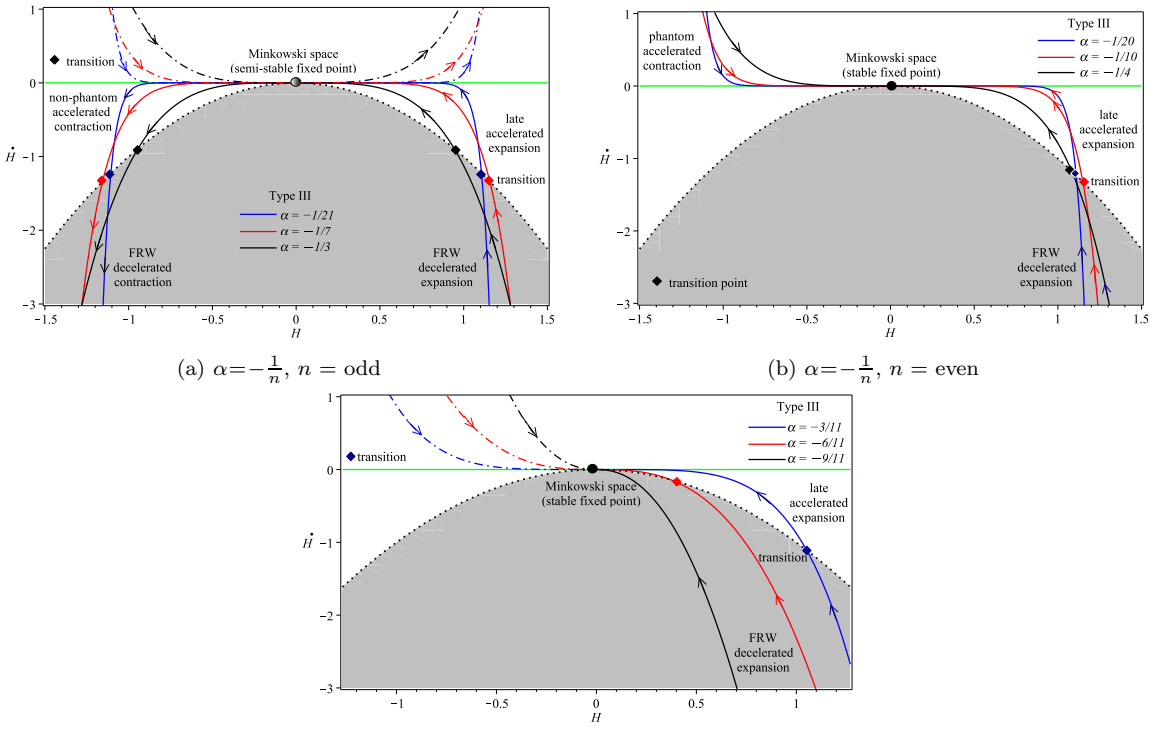

(a) $\alpha=-\frac{1}{n}$, n = odd

(b) $\alpha=-\frac{1}{n}$, n = even

(c) $\alpha=-\frac{a}{b}$, $a<b$ and $\frac{a}{b}\neq\frac{1}{n}$

Fig. 4. (color online) Phase portraits of finite-time singularities of Type III for different choices of the parameter $-1<\alpha<0$ in Eq. (8). The dashed curves correspond to $f_0<0$ ($\beta<0$), and the solid curves correspond to $f_0>0$ ($\beta>0$). Same-color curves show the same value of α. The phase portraits of (b) are typical for both $\beta<0$ and $\beta>0$.

In this case, the Minkowskian fixed point is stable (attractor), and therefore the $H<0$ and $H>0$ regions are separated by an infinite time. Therefore, we discuss each as a separate region. In the positive H region, the cosmic behavior is the same as in case 1. However, in the negative H region, the universe evolves effectively in the phantom regime. It begins with a finite-time singularity at $t_s=(H_0/\beta)^{1/\alpha}$, then it evolves towards the right (increasing H). So the universe experiences an eternal accelerated contraction phase with a Minkowskian fate at an infinite time, i.e. it has no future singularity.

Case 3. $\alpha=-\frac{a}{b}$ (a and b are positives, and $a<b$ but $\frac{a}{b}\neq\frac{1}{n}$): The corresponding phase portraits are indicated by the dashed curves in Fig. 4(c). Remarkably, the positive H region is not valid in this case. On the other hand, the dynamical behavior of the universe is the same as in cases 1 and 2 above, in the $H<0$ region.

2.3.2 $f_0>0$ ($\beta>0$)

In this category, similarly, three patterns can be obtained, depending on the value of α. Therefore, we have the following subclasses.

Case 1. $\alpha=-\frac{1}{n}$ ($n>1$ is an odd positive integer): The phase portraits for some particular choices of α are indicated by the solid curves in Fig. 4(a), where the Minkowskian fixed point at the origin of the phase space is a common point for all portraits. The Minkowski space, in this case, is a semi-stable fixed point. Since the universe requires an infinite time to reach this Minkowskian space, we find that $H>0$ and $H<0$ are two separate regions. Firstly, we discuss the $H>0$ region, where the universe evolves in the decreasing H direction. As shown by the plots, the universe has an initial finite-time singularity with a decelerated expansion behavior, where the age of the universe, for some value $H_0>0$, can be given by

$$t_s=\int_{\infty}^{H_0}\frac{\mathrm{d}H}{\dot{H}}=\left(\frac{H_0}{\beta}\right)^{1/\alpha}.$$

However, for a proper choice of the parameters α and β, the universe can evolve from deceleration to acceleration phase. If we assume that the transition has occurred at some value $H_{de}>0$, then the phase portrait should cut the zero acceleration curve (i.e. $\dot{H}=-H^2$) at that value. Using Eq. (8), at the transition point, the two parameters can be related by

$$\beta=H_{de}\left(-\frac{H_{de}}{\alpha}\right)^{\alpha}. \tag{12}$$

For any value of $-1<\alpha<0$, the above equation can predict the value of β when the Hubble parameter (or the

red-shift) at transition is accurately measured by observations. For more detailed discussion about the possible values of α and β to realize that transition, see Section 2.5. As shown in Fig. 4(a), the universe evolves towards quasi-de Sitter, i.e. $\omega_{\rm eff}\to -1$, with a Minkowskian fate, which is unusual when dark energy is interpreted as a cosmological constant. Secondly, we discuss the $H<0$ region, where the universe evolves in the decreasing H direction. As shown by the plots, the universe evolves from the Minkowskian fixed point, so it has no initial finite-time singularity. However, it begins with an accelerated contraction, then enters a later decelerated contraction with a future finite-time singularity at $t_s=-\left|\frac{H_0}{\beta}\right|^{1/\alpha}$ from some value $H_0<0$. Similarly, in this region, the transition from an accelerated to a decelerated contraction can be realized. In this case, if we assume a negative cosmological constant in Eq. (8), we expect the phase portrait to shift downwards, avoiding the Minkowskian fixed point, where a turnaround cosmology occurs.

Case 2. $\alpha=-\frac{1}{n}$ ($n>1$ is an even positive integer): The corresponding phase portraits are given in Fig. 4(b). As mentioned in Section 2.3.1, the phase portraits of $\pm\,\beta$ are identical. Therefore, we expect the same description as given before.

Case 3. $\alpha=-\frac{a}{b}$ (a and b are positives, and $a<b$ but $\frac{a}{b}\neq\frac{1}{n}$): The corresponding phase portraits are indicated by the solid curves in Fig. 4(c). Remarkably, the negative H region is not valid in this case. On the other hand, the positive H region is valid, and the dynamical evolution is just as in cases 1 and 2.

2.3.3 Physical description

In conclusion, we find that the choice of $\beta>0$ provides an alternative to the ΛCDM models. In this scenario, the universe begins with an initial singularity of Type III, instead of the Type I of the standard cosmology (big bang). Then, the universe traverses from deceleration to acceleration. However, it evolves towards a Minkowskian fate, not de Sitter, which is distinguishable from ΛCDM models when the dark energy is interpreted as a cosmological constant. In Section 4.3, we provide a complementary study through torsion gravity to explain the late accelerating expansion phase of the model.

2.4 Type IV singularity phase portrait

This singularity occurs when the cosmic time approaches $t\to t_s$. All three quantities, a, $\rho_{\rm eff}$ and $|p_{\rm eff}|$, approach finite values, i.e. $a\to a_s$, $\rho_{\rm eff}\to\rho_s$ and $|p_{\rm eff}|\to p_s$. In addition, the Hubble parameter and its first derivative are finite, while its second/higher derivatives diverge. The Type IV singularity is the softest (not of the crushing type) of four types, c.f. Refs. [10, 22, 25, 29–31]. Using the scale factor (5), the Type IV singularity case occurs when $\alpha>1$. In this case, similar to the Type I singularity, we have $\beta=f_0(1+\alpha)<0$, when $f_0>0$, while $\beta=f_0(1+\alpha)>0$, when $f_0<0$. Different cases of the phase portraits corresponding to Eq. (8) are given in Fig. 5. Although the singularity of Type IV is a fixed point as well, as appears in the phase portrait, it can be reached in a finite time. This argument can be verified as follows. Since, in the Type IV case, the singularity occurs when the higher derivatives of the Hubble rate are divergent as $H\to H_s$, this means that

$$\lim_{H\to H_s}\frac{{\rm d}^nH}{{\rm d}t^n}=\pm\infty,$$

for some $n\geqslant 2$. Let us compute the lowest derivative for which the Type IV singularity could occur, which is for $n=2$,

$$\lim_{H\to H_s}\ddot{H}=\lim_{H\to H_s}\dot{H}\left(\frac{{\rm d}\dot{H}}{{\rm d}H}\right)=\pm\infty.$$

Since $\dot{H}$ is finite, it implies that

$$\lim_{H\to H_s}\frac{{\rm d}\dot{H}}{{\rm d}H}=\pm\infty. \tag{13}$$

This can be shown graphically on the phase space, Fig. 5, as an infinite slope of the phase portrait at the Type IV singularity phase point. Remarkably, this type of singularity is the only one of the four which coincides with a fixed point. In general, fixed points dominate one-dimensional autonomous systems, where the time required to reach these points is infinite, as shown by Eq. (10). However, Type IV singularities are exceptions and the system can reach them in a finite time. In order to clarify this point, we rewrite the Friedmann equation (2) as

$$\dot{H}=-\frac{\kappa^2}{2}(p_{\rm eff}+\rho_{\rm eff}).$$

It has been shown that for an equation of state $p_{\rm eff}(H)$, where the pressure is continuous and differentiable, the solution always reaches a fixed point in an infinite time [32]. This leaves us with the other option where the pressure is not differentiable, i.e. ${\rm d}p_{\rm eff}/{\rm d}H$ is not continuous. In this case, we can also have two possible cases. The first is when the discontinuity of ${\rm d}p_{\rm eff}/{\rm d}H$ is finite, and the time to reach a fixed point is infinite. The second case is when ${\rm d}p_{\rm eff}/{\rm d}H$ is infinite discontinuous, and is the only possible option to reach a fixed point in a finite time[1)]. Since $\rho_{\rm eff}\sim H^2$, we see that ${\rm d}p_{\rm eff}/{\rm d}H$ is infinite discontinuous if ${\rm d}\dot{H}/{\rm d}H$ diverges. Therefore, we write the following conditions for a fixed point H_f to be reached in a finite time:

(i) $\lim_{H\to H_f}\dot{H}=0$,

1) In the general relativistic picture, condition (13) leads to a divergence of the speed of sound ${\rm d}p_m/{\rm d}\rho_m=c_s^2$, so the solution will not be causal.

(ii) $\lim_{H\to H_f} \mathrm{d}\dot{H}/\mathrm{d}H=\pm\infty$,

(iii) $t=\int_H^{H_f} \mathrm{d}H/\dot{H}<\infty$.

The above conditions are always fulfilled in the case of finite-time singularities of Type IV. Although the above calculations have been carried out for the lowest divergent derivatives $\ddot{H}\to\pm\infty$, they can be generalized for other higher lowest divergent derivatives of the Hubble parameter. We next turn our discussions of the phase portraits associated with singularities of Type IV for some particular values of the model parameters α and β.

2.4.1 $f_0>0$ ($\beta<0$)

The corresponding phase portraits are indicated by the solid curves in Fig. 5. The universe has an initial singularity of Type IV at the Minkowskian unstable fixed point, and then it evolves in a phantom regime. Although the phase portrait evolves towards $H\to\infty$, it will not have a future finite-time singularity, as clarified earlier after Eq. (8).

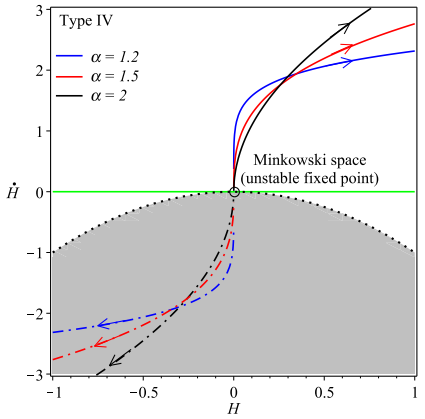

Fig. 5. Phase portraits of finite-time singularities of Type IV for different choices of the parameter $\alpha>1$ in Eq. (8). The solid curves correspond to $f_0>0$ ($\beta<0$), and the dashed curves correspond to $f_0<0$ ($\beta>0$). Same-color curves show the same value of α.

2.4.2 $f_0<0$ ($\beta>0$)

The corresponding phase portraits are indicated by the dashed curves in Fig. 5. The universe begins with a finite-time singularity of Type IV at a Minkowskian unstable fixed point, then it evolves in a non-phantom regime. It evolves towards $H\to-\infty$ with an early decelerated contraction phase. The universe then enters a later accelerating contraction phase. Although the phase portrait evolves towards a big crunch singularity, it cannot be reached in a finite time, as clarified before. Therefore, the universe will not have a future finite-time singularity.

2.4.3 Physical description

In conclusion, we mention that the universe takes an infinite time to leave or to reach a fixed point. So if the universe begins at a fixed point, it stays forever at that point. However, singularities of Type IV allow the universe to leave or to reach fixed points in a finite time, so these types of singularities may provide an important key in inflationary models. In addition, if the phase portrait is double valued about a Type IV singularity, the universe is capable of crossing the phantom divide line. The latter situation provides important dynamical features in bouncing cosmologies.

In the case at hand, which is shown in Fig. 5, the plots show that the cosmic fluid flow is towards the right (increasing H), whereas the Minkowskian fixed point coincides with the singular point of Type IV. The time to reach the initial singularity is $t=\left(\frac{H_0}{\beta}\right)^{1/\alpha}$ for a some value H_0. On the other hand, the universe has no future singularity, as the time required to approach $H\to\infty$ is infinite.

2.5 General remarks

As shown in the previous sections, phase portrait analysis is a powerful qualitative tool to extract dynamical information by fitting all possible universes on a small piece of paper. In this section, we summarize some general conclusions which characterize the dynamical evolution associated with each finite-time singularity type. In addition, we extract some useful quantitative information to conform the evolution to some important cosmic events. We noted that transition from acceleration to deceleration, see Section 2.1, or from deceleration to acceleration, see Section 2.3, could be realized for $H>0$ only in Type I or Type III singularities, respectively. This conclusion can be clearly seen using Fig. 6(a).

Type I ($\alpha<-1$): For $f_0<0$ ($\beta>0$), the transition from acceleration to deceleration is allowed, see Fig. 2(b). So this model is suitable to describe graceful exit inflationary models, where the universe begins with a big bang inflation, then it exits into a decelerated FLRW phase. Since we deal with high energy scales, it is convenient to measure the Hubble parameter in Planck units. We assume that inflation ends at $10^{-34}\lesssim t\lesssim 10^{-31}$ s, i.e. $10^7\lesssim H_{\rm inf}\lesssim 10^9$ GeV. Substituting into Eq. (11), we obtain the values of (α, β) which allow a viable graceful exit inflation. We represent the solution graphically in Fig. 6(b).

Type II ($0<\alpha<1$): For particular choices of $\alpha=\frac{1}{n}$, where n is a positive odd integer, we have a bouncing cosmology with a singularity of type II at the bouncing time, see Fig. 3(a). Here junction conditions should be used to weld the contraction and the expansion phases. In order to avoid the trans-Planckian problem of inflationary model, it is convenient to choose the finite value

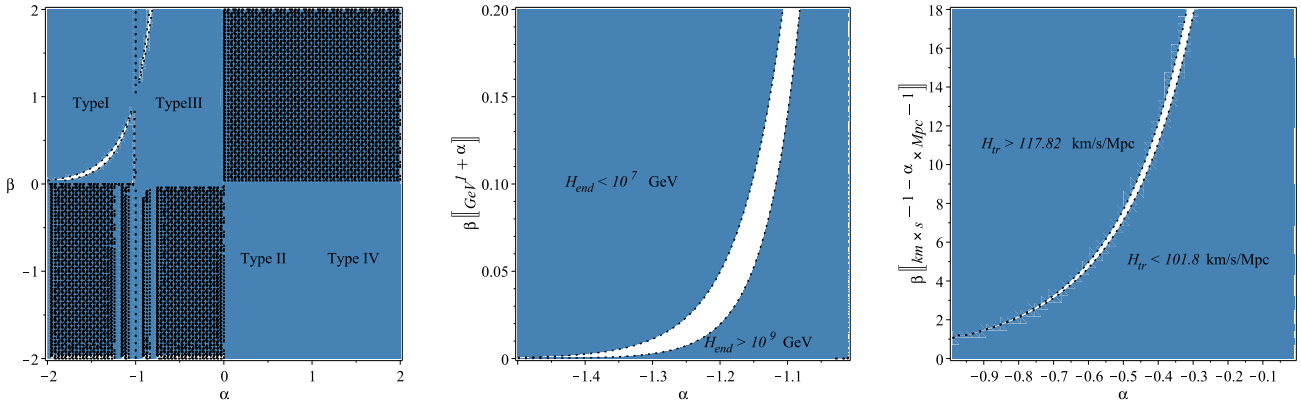

(a) Full range of four singularity types (b) Type I (c) Type III

Fig. 6. (color online) (a) (α, β) diagram shows the values which allow transitions (11) and (12), and the dark regions are forbidden values, the blue regions are excluded values, while the white regions are accepted values. (b) Values of the parameters α and β which allow transition from acceleration to deceleration at $10^7 \lesssim H_{\rm inf} \lesssim 10^9$ GeV, with the dotted curves showing the values of α and β which allow transition at $H_{\rm inf}=10^7$ and 10^9 GeV exactly. (c) Values of the parameters α and β which allow transition from deceleration to acceleration at redshift $0.72 \lesssim z_{de} \lesssim 0.84$ (i.e. $101.8 \lesssim H_{de} \lesssim 117.82$ km/s/Mpc), with the dotted curves showing the values of α and β which allow transition at $H_{de}=101.8$ and 117.82 km/s/Mpc exactly.

ρ_m to be at the Planckian density limit, or the minimal Hubble parameter to have the Planck length. In this case we would have a non-singular bouncing scenario that can avoid the trans-Planckian problems of the inflationary models.

Type III $(-1<\alpha<0)$: We noted that the transition from deceleration to acceleration, in the $H>0$ region, can be achieved, so this model provides an alternative to the ΛCDM universe. However, it evolves towards a Minkowskian rather than a de Sitter universe, which is unusual when dark energy is interpreted as a cosmological constant. In general, if the red-shift at transition (or the Hubble value H_{de}) is accurately measured by observations, we can solve Eq. (12) to obtain viable solutions of (α, β). Since we deal with low energy scales, it is convenient to measure the Hubble parameter in SI units[1] [km/s/Mpc]. A recent analysis [36] shows that the deceleration to acceleration transition is at $z_{de}=0.72\pm0.05$ (0.84 ± 0.03) when the present Hubble constant is taken as $H_0=68\pm2.8$ (73.24 ± 1.74) km/s/Mpc. We provide a graphical solution in Fig. 6 by assuming that the transition occurs in the range $101.8<H_{de}<17.82$ km/s/Mpc.

Type IV $(\alpha>1)$: Remarkably, the singular point in this model is a repeller fixed point as well. Usually, the universe takes an infinite time to reach that point. However, in a Type IV singularity the higher derivative of the Hubble parameter diverges. Consequently, we have $\mathrm{d}\dot{H}/\mathrm{d}H \to \pm\infty$. This provides a unique case, that is, the fixed point can be reached in a finite time. So we may use this model to cross the phantom divide line between phantom and non-phantom regimes, if the phase portrait is a double valued function about the fixed point.

As shown in the above discussion, phase space analysis is a useful tool to understand the evolution of the universe in a clear and transparent way. However, we also need to reformulate this description within a field theory framework for better understanding.

3 Generalized teleparallel gravity

In general relativity (GR), the Friedmann system provides a power law scale factor, if we assume that the matter content is a perfect fluid with a linear (fixed) equation of state parameter ω_m such that $0 \leqslant \omega_m \leqslant 1$, to guarantee the stability and causality conditions. Otherwise, one needs to assume that the matter content has an exotic equation of state, c.f. Refs. [31, 32, 37]. In fact, the power law scale factor can predict perfectly the thermal history during radiation/matter dominant eras. However, it fails to describe the early and the late accelerating expansion epochs. In this sense, modified gravity may explain these epochs by modifying the gravitational sector.

However, as we clarified earlier, phase portrait analysis through the stability of its fixed points requires the Friedman equations to be written as a one-dimensional autonomous system. Among several extensions of GR, we note that its teleparallel equivalent version (TEGR), c.f. Ref. [38], and its $f(T)$ extension, have features which

1) Remember that 1 Mpc = 3.09 × 10^{19} km, so the quantity km/Mpc is dimensionless. Consequently, the Hubble parameter is measured in $[\mathrm{s}]^{-1}$.

make them compatible with our phase portrait analysis [33]. That is, the teleparallel torsion is proportional to the quadratic Hubble parameter so that the modified gravitational sector does not introduce the second or any higher derivatives of the Hubble parameter. For other extensions of teleparallel gravity see Refs. [39–42]. Since the modified Friedmann equations according to $f(T)$ gravity contain only the Hubble parameter and its rate of change, it is consistent with the phase space analysis. Therefore, the $f(T)$ theories, among many modified gravity theories, can be considered as a natural extension to GR.

3.1 Teleparallel space

In Riemannian space of n dimensions, the metric tensor field $g_{\mu\nu}$ is the fundamental quantity. In Weitzenböck space of n dimensions[1)], the vielbein vector field ${e_a}^{\mu}$ is the fundamental quantity. The latter can be defined as a pair (M,e_a), where M is an n-dimensional differentiable manifold and the set $\{e_a\}$ contains n independent vector fields defined globally on M. This set at point p is the basis of its tangent space T_pM. Because of the independence of e_a, the determinant $e\equiv\det({e_a}^{\mu})$ is nonzero. Then, one can define the linear (Weitzenböck) connection

$$\Gamma^{\alpha}{}_{\mu\nu}\equiv{e_a}^{\alpha}\partial_{\nu}{\rm e}^{a}{}_{\mu}=-{\rm e}^{a}{}_{\mu}\partial_{\nu}{e_a}^{\alpha}. \tag{14}$$

This connection is characterized by the property that

$$\nabla_{\nu}{e_a}^{\mu}\equiv\partial_{\nu}{e_a}^{\mu}+\Gamma^{\mu}{}_{\lambda\nu}{e_a}^{\lambda}\equiv 0, \tag{15}$$

where the covariant derivative ∇_{ν} is associated with the Weitzenböck connection. This nonsymmetric connection uniquely determines the teleparallel geometry, since the vielbein vector fields are parallel with respect to it. Indeed, a vielbein space admits the dual and the symmetric connections associated with the Weitzenböck, except they do not provide a teleparallel geometry. For more details about these connections and their applications see Refs. [43–52]. Also, for more details of the parameterized versions of these connections and their applications see Refs. [53–61]. However, the vielbein vector fields satisfy

$${e_a}^{\mu}{\rm e}^{a}{}_{\nu}=\delta^{\mu}_{\nu}\quad\text{and}\quad{e_a}^{\mu}{\rm e}^{b}{}_{\mu}=\delta^{b}_{a}, \tag{16}$$

where δ is the Kronecker tensor. Thus, we can construct an associated (pseudo-Riemannian) metric for any set of basis

$$g_{\mu\nu}\equiv\eta_{ab}{\rm e}^{a}{}_{\mu}{\rm e}^{b}{}_{\nu}, \tag{17}$$

while the inverse metric

$$g^{\mu\nu}=\eta^{ab}{e_a}^{\mu}{e_b}^{\nu}. \tag{18}$$

Also, it can be shown that $e=\sqrt{-g}$, where $g\equiv\det(g)$. In this sense, the vielbein space is pseudo-Riemannian as well. Thus, we go further to define the symmetric Levi-Civita connection

$$\mathring{\Gamma}^{\alpha}{}_{\mu\nu}=\frac{1}{2}g^{\alpha\sigma}(\partial_{\nu}g_{\mu\sigma}+\partial_{\mu}g_{\nu\sigma}-\partial_{\sigma}g_{\mu\nu}). \tag{19}$$

Recalling the absolute parallelism condition (15), it is easy to show that the Weitzenböck and the Levi-Civita connections are both metric connections, i.e.

$$\nabla_{\sigma}g_{\mu\nu}\equiv 0,\quad\mathring{\nabla}_{\sigma}g_{\mu\nu}\equiv 0,$$

where $\mathring{\nabla}_{\nu}$ is the covariant derivative associated with the Levi-Civita connection.

The noncommutation of an arbitrary vector field V_a is given by

$$\begin{aligned}\nabla_{\nu}\nabla_{\mu}{V_a}^{\alpha}-\nabla_{\mu}\nabla_{\nu}{V_a}^{\alpha}&=R^{\alpha}{}_{\epsilon\mu\nu}{V_a}^{\epsilon}+T^{\epsilon}{}_{\nu\mu}\nabla_{\epsilon}{V_a}^{\alpha},\\ \mathring{\nabla}_{\nu}\mathring{\nabla}_{\mu}{V_a}^{\alpha}-\mathring{\nabla}_{\mu}\mathring{\nabla}_{\nu}{V_a}^{\alpha}&=\mathring{R}^{\alpha}{}_{\epsilon\mu\nu}{V_a}^{\epsilon}+\mathring{T}^{\epsilon}{}_{\nu\mu}\mathring{\nabla}_{\epsilon}{V_a}^{\alpha},\end{aligned}$$

where $R^{\alpha}{}_{\epsilon\mu\nu}$ ($\mathring{R}^{\alpha}{}_{\epsilon\mu\nu}$) and $T^{\epsilon}{}_{\nu\mu}$ ($\mathring{T}^{\epsilon}{}_{\nu\mu}$) are the curvature and torsion tensors of the Weitzenböck (Levi-Civita) connection, respectively. The absolute parallelism condition (15) and the noncommutation formula force the curvature tensor $R^{\alpha}{}_{\mu\nu\sigma}$ of the Weitzenböck connection to vanish identically, i.e. $R^{\alpha}{}_{\epsilon\mu\nu}\equiv 0$, while the symmetric Levi-Civita connection provides a vanishing torsion tensor, i.e. $\mathring{T}^{\epsilon}{}_{\nu\mu}\equiv 0$.

The torsion tensor of the Weitzenböck connection (14) is defined as

$$T^{\alpha}{}_{\mu\nu}\equiv\Gamma^{\alpha}{}_{\nu\mu}-\Gamma^{\alpha}{}_{\mu\nu}={e_a}^{\alpha}(\partial_{\mu}{\rm e}^{a}{}_{\nu}-\partial_{\nu}{\rm e}^{a}{}_{\mu}). \tag{20}$$

Then, the contortion tensor $K^{\alpha}{}_{\mu\nu}$ is defined by

$$K^{\alpha}{}_{\mu\nu}\equiv\Gamma^{\alpha}{}_{\mu\nu}-\mathring{\Gamma}^{\alpha}{}_{\mu\nu}={e_a}^{\alpha}\,\mathring{\nabla}_{\nu}{\rm e}^{a}{}_{\mu}. \tag{21}$$

$T_{\mu\nu\sigma}$ is skew symmetric in the last pair of indices whereas $K_{\mu\nu\sigma}$ is skew symmetric in the first pair of indices. Moreover, the torsion and the contortion can be interchanged following the useful relations:

$$T_{\alpha\mu\nu}=K_{\alpha\mu\nu}-K_{\alpha\nu\mu}, \tag{22}$$

$$K_{\alpha\mu\nu}=\frac{1}{2}(T_{\nu\alpha\mu}+T_{\alpha\mu\nu}-T_{\mu\alpha\nu}). \tag{23}$$

In teleparallel space there are three Weitzenböck invariants: $I_1=T^{\alpha\mu\nu}T_{\alpha\mu\nu}$, $I_2=T^{\alpha\mu\nu}T_{\mu\alpha\nu}$ and $I_3=T^{\alpha}T_{\alpha}$, where $T^{\alpha}=T_{\rho}{}^{\alpha\rho}$. We next define the invariant

$$T=\frac{1}{4}I_1+\frac{1}{2}I_2-I_3,$$

by combining the three invariants I_1, I_2 and I_3 with the prefixes coefficients as appears above. This teleparallel invariant is equivalent to the Ricci scalar $\mathring{R}$ up to a total derivative term, as we will show below. Alternatively, the teleparallel torsion scalar is given in the compact form

$$T\equiv T^{\alpha}{}_{\mu\nu}S_{\alpha}{}^{\mu\nu}, \tag{24}$$

1) The Latin indices are the Lorentz indices and the Greek indices are the coordinate indices, where both run from $1,\cdots,n$ and additionally follow the Einstein summation convention.

where the superpotential tensor,

$$S_\alpha{}^{\mu\nu}=\frac{1}{2}\left(K^{\mu\nu}{}_\alpha+\delta^\mu_\alpha T^{\beta\nu}{}_\beta-\delta^\nu_\alpha T^{\beta\mu}{}_\beta\right), \tag{25}$$

is skew symmetric in the last pair of indices. Indeed, we deal with exactly one space. However, Levi-Civita and Weitzenböck connections can see this space with different resolutions. The former represents an extreme picture with a vanishing torsion tensor, while the latter represents another extreme with a vanishing curvature tensor. Interestingly, one can find possible links between these two extremes. Thus, a useful link in this context is the following identity:

$$e\mathring{R}\equiv -eT+2\partial_\mu(eT^\mu), \tag{26}$$

where the divergence term is sometimes given in terms of the Levi-Civita covariant derivative as $\partial_\mu(eT^\mu)=e\mathring{\nabla}_\mu T^\mu$. Since the Ricci and the teleparallel torsion scalars differ by a total derivative term, both would provide the same set of field equations using the Lagrangian formalism, GR, and TEGR. Although superficially equivalent on the level of the field equations, the difference runs deep on the Lagrangian level. It can be shown that the left-hand side of the geometrical identity (26) is a diffeomorphism scalar and Lorentz as well. However, the total derivative term on the right-hand side is not a Lorentz scalar. Consequently, the teleparallel torsion scalar density is a diffeomorphism scalar but not a Lorentz scalar. This contrast is crucial in the generalization of the Lagrangian of the GR and TEGR theories by taking, respectively, $f(\mathring{R})$ and $f(T)$ extensions. The former provides field equations invariant under local Lorentz transformation, while the latter does not [62–65]. We consider the action of the $f(T)$ gravity [66, 67]

$$\mathcal{S}=\frac{1}{2\kappa^2}\int \mathrm{d}^4x\; ef(T)+\mathcal{S}_m, \tag{27}$$

where $\mathcal{S}_\Updownarrow$ is the matter action. The variation of the action (27) with respect to the tetrad gives

$$\begin{aligned}&\frac{1}{e}\partial_\mu(eS_a{}^{\mu\nu})f'-e^\lambda_a T^\rho{}_{\mu\lambda}S_\rho{}^{\nu\mu}f'\\&+S_a{}^{\mu\nu}\partial_\mu T f''+\frac{1}{4}e^\nu_a f=\frac{\kappa^2}{2}e^\rho_a\mathfrak{T}_\rho{}^\nu,\end{aligned} \tag{28}$$

where $f=f(T)$, $f'=\frac{\partial f(T)}{\partial T}$, $f''=\frac{\partial^2 f(T)}{\partial T^2}$, and $\mathfrak{T}_\mu{}^\nu$ is the usual energy-momentum tensor of matter fields. It is clear that the field equations (28) reproduce the TEGR theory by setting $f(T)=T$. The $f(T)$ modified gravity theories have been used widely in literature in cosmology [20, 21, 23, 68–79], and in astrophysical applications [80–90]. For more details about $f(T)$ gravity see the review in Ref. [91].

3.2 Reconstructing $f(T)$

We consider the diagonal vierbein corresponding to the FLRW metric (1), i.e.

$$e_\mu{}^a=\mathrm{diag}(1,a(t),a(t),a(t)). \tag{29}$$

This directly relates the teleparallel torsion scalar (24) to the Hubble parameter as

$$T=-6H^2. \tag{30}$$

The useful relation above facilitates many cosmological applications in $f(T)$ gravity. We assume that the stress-energy tensor for perfect fluid is

$$\mathfrak{T}_{\mu\nu}=\rho_m u_\mu u_\nu+p_m(u_\mu u_\nu-g_{\mu\nu}), \tag{31}$$

where u^μ is the fluid 4 velocity, and ρ_m and p_m are the energy density and pressure respectively of the fluid in its rest frame. Inserting the vierbein (29) into the field equations (28) for the matter fluid (31), the modified Friedmann equations of the $f(T)$-gravity read

$$\rho_m = \frac{1}{2\kappa^2}[f(T)+12H^2f_T], \tag{32}$$

$$p_m = \frac{-1}{2\kappa^2}\left[f(T)+4(3H^2+\dot{H})f_T-48\dot{H}H^2f_{TT}\right]. \tag{33}$$

In the above, the usual Friedmann equations are recovered by setting $f(T)=T$. Assuming that the matter fluid is governed by the linear equation of state $p_m=\omega_m\rho_m$, where $\omega_m=0$ for dust and $\omega_m=1/3$ for radiation, the system acquires the conservation (continuity) equation

$$\dot{\rho}_m+3H(1+\omega_m)\rho_m=0. \tag{34}$$

As mentioned before, the modified Friedmann equations of any $f(T)$-theory can be viewed as a *one-dimensional autonomous system*, i.e. $\dot{H}=\mathcal{F}(H)$, if we use the linear equation of state of the universe matter. So it is convenient now to represent Eqs. (32) and (33) in terms of H [33],

$$\rho_m = \frac{1}{2\kappa^2}[f(H)-Hf_H], \tag{35}$$

$$p_m = \frac{-1}{2\kappa^2}\left[f(H)-Hf_H-\frac{1}{3}\dot{H}f_{HH}\right], \tag{36}$$

where $f_H:=\frac{\mathrm{d}f}{\mathrm{d}H}$ and $f_{HH}:=\frac{\mathrm{d}^2f}{\mathrm{d}H^2}$. After some manipulation, we write

$$\dot{H}=3(1+\omega_m)\left[\frac{f(H)-Hf_H}{f_{HH}}\right]=\mathcal{F}(H). \tag{37}$$

Combining (8) and (37), we can obtain the $f(H)$ which produces some desired phase trajectory. The integral of the continuity equation (34) can be given by

$$\rho_m=\rho_{m,0}\;\mathrm{e}^{-3(1+\omega_m)\int\frac{H}{\dot{H}}\mathrm{d}H}, \tag{38}$$

where the integration constant

$$\rho_{m,0}\equiv\rho_m(t_0)\approx 1.88\times10^{-26}\;\Omega_{m,0}\;h_0^2\;\mathrm{kg/m^3},$$

and the matter density parameter $\Omega_{m,0}$, and the dimensionless Hubble constant h_0 are given by the observations at present time t_0. Substituting (8) into (38), then Eq. (35) reads

$$f(H)-Hf_H=2\kappa^2\rho_{m,0}\,\mathrm{e}^{-\frac{3(1+\omega_m)H}{-1+\alpha}\left(\frac{H}{\beta}\right)^{-1/\alpha}}.$$

Solving the above equation with respect to $f(H)$, we obtain

$$f(H) = A\left[B\ \mathrm{WhittakerM}\left(\frac{-2\alpha-1}{2+2\alpha},\frac{2+\alpha}{2+2\alpha},\frac{-C}{1+\alpha}\right)+\frac{1}{3}\ \mathrm{WhittakerM}\left(\frac{1}{2+2\alpha},\frac{2+\alpha}{2+2\alpha},\frac{-C}{1+\alpha}\right)\right], \quad (39)$$

where A, B and C are functions of the Hubble parameter, which can be listed as follows

$$A\equiv A(H) = \frac{6\rho_{m,0}\kappa^2}{2+\alpha}\left[\frac{1+\alpha}{3(1+\omega_m)}\right]^{\frac{3+2\alpha}{2+2\alpha}}\times H^{-\frac{3+2\alpha}{2\alpha}}\beta^{\frac{3+2\alpha}{2\alpha(1+\alpha)}}\mathrm{e}^{\frac{C}{2+\alpha}}, \quad (40)$$

$$B\equiv B(H) = \frac{1+\alpha}{3}(1-C), \quad (41)$$

$$C\equiv C(H) = -3\beta(1+\omega_m)H\left(\frac{H}{\beta}\right)^{\frac{1}{\alpha}}. \quad (42)$$

We note that in Eq. (39), we omitted a term $H\propto\sqrt{-T}$, because it has no contribution to the field equations. So we omit this term without losing the generality of the solution. Substituting (39) into (35) and (36), the density and pressure of the matter fluid read

$$\rho_m(H) = \rho_{m,0}\mathrm{e}^{-\frac{3(1+\omega_m)H}{1+\alpha}\left(\frac{H}{\beta}\right)^{\frac{1}{\alpha}}}, \quad (43)$$

$$p_m(H) = \omega_m\rho_{m,0}\mathrm{e}^{-\frac{3(1+\omega_m)H}{1+\alpha}\left(\frac{H}{\beta}\right)^{\frac{1}{\alpha}}}. \quad (44)$$

By evaluating the density and the pressure of the ordinary matter, we can provide a complementary description of the cosmic evolution by identifying the gravitational sector contribution, which in our case is the torsion contribution.

4 The role of torsion

In order to show the role of torsion in cosmic evolution near the singularities, it is convenient to transform Eqs. (35) and (36) from the *matter* frame to the *effective* frame in which the equations would have the standard Einstein's field equations in addition to the torsion contribution as a higher order gravity of the $f(T)$ theory. We write the modified Friedmann equations in the case of $f(T)$ gravity as:

$$H^2 = \frac{\kappa^2}{3}(\rho_m+\rho_T) \equiv\frac{\kappa^2}{3}\rho_{\mathrm{eff}}, \quad (45)$$

$$2\dot{H}+3H^2 = -\kappa^2(p_m+p_T)\equiv-\kappa^2 p_{\mathrm{eff}}, \quad (46)$$

where ρ_T and p_T are the effective density and pressure of the torsion fluid, respectively. By comparison with Eqs. (35) and (36) we write

$$\rho_T(H) = \frac{1}{2\kappa^2}[Hf_H-f(H)+6H^2], = \frac{3}{\kappa^2}H^2-\rho_{m,0}\mathrm{e}^{-\frac{3(1+\omega_m)H}{1+\alpha}\left(\frac{H}{\beta}\right)^{\frac{1}{\alpha}}}. \quad (47)$$

$$p_T(H) = -\frac{1}{6\kappa^2}\dot{H}(12+f_{HH})-\rho_T(H), = -\frac{1}{\kappa^2}\left[3H^2+2\alpha H\left(\frac{\beta}{H}\right)^{\frac{1}{\alpha}}\right] -\omega_m\rho_{m,0}\mathrm{e}^{-\frac{3(1+\omega_m)H}{1+\alpha}\left(\frac{H}{\beta}\right)^{\frac{1}{\alpha}}}. \quad (48)$$

In the above we have replaced the value of $\dot{H}$ from Eq. (37). One can show that ρ_T and p_T vanish where $f(H)=-6H^2$ and the standard Friedmann equations are recovered. In this case the effective torsion gravity acquires the conservation equation

$$\dot{\rho}_T+3H[1+\omega_T(H)]\rho_T\equiv0. \quad (49)$$

We first evaluate the effective equation of state parameter. Using Eq. (8), we obtain

$$\omega_{\mathrm{eff}} \equiv \frac{p_m+p_T}{\rho_m+\rho_T}=-1-\frac{2\dot{H}}{3H^2}, = -1-\frac{2}{3}\frac{\alpha}{H}\left(\frac{\beta}{H}\right)^{\frac{1}{\alpha}}. \quad (50)$$

It is convenient to study the asymptotic behavior at large Hubble regimes where $H\to\pm\infty$. In general, for the power-law phase portraits $\dot{H}\propto H^\gamma$, we have $\omega_{\mathrm{eff}}\to-1$ where $\gamma<2$, while $\omega_{\mathrm{eff}}\to\pm\infty$ where $\gamma>2$. Also, we investigate the behavior of the effective equation of state at the Minkowskian fixed point $H=0$. We find that $\omega_{\mathrm{eff}}\to\pm\infty$ where $\gamma<2$, while $\omega_{\mathrm{eff}}\to-1$ where $\gamma>2$. For the model at hand, by recalling Eq. (50), at the limit $H\to\pm\infty$, we have the case of $\omega_{\mathrm{eff}}\to-1$ where $\alpha<-1$ or $\alpha>0$, which covers the singularities of Types I, II and IV. For the same range, $\alpha<-1$ or $\alpha>0$, at the limit $H\to0$, we obtain the following

$$\lim_{H\to0}\omega_{\mathrm{eff}}=Q_0,\quad \lim_{H\to\pm\infty}\omega_{\mathrm{eff}}=-1, \quad (51)$$

where $Q_0\equiv Q_0(H)=-\frac{2}{3}\frac{\alpha}{H}\left(\frac{\beta}{H}\right)^{1/\alpha}$. However, for the range $-1<\alpha<0$, it is easy to verify that the effective equation of state having the following limits

$$\lim_{H\to0}\omega_{\mathrm{eff}}=-1,\quad \lim_{H\to\pm\infty}\omega_{\mathrm{eff}}=Q_0, \quad (52)$$

which describes the cosmic evolution associated with the Type III singularity. In conclusion, the effective equation of state evolves towards either -1 or $\pm\infty$. We summarize the behavior of the effective fluid in Table 2 in Section 5.

We next turn the discussion to the dynamical description instead of the above kinematical one. Therefore, we investigate the torsion role near the singularities using the torsion equation of state parameter, that is

$$\omega_T \equiv \frac{p_T}{\rho_T}=-1+\frac{1}{3}\frac{\dot{H}(12+f_{HH})}{f(H)-6H^2-Hf_H},$$
$$=-1+\frac{2\alpha H(\beta/H)^{\frac{1}{\alpha}}\mathrm{e}^{\frac{3(1+\omega_m)H}{(1+\alpha)}\left(\frac{H}{\beta}\right)^{\frac{1}{\alpha}}}-(1+\omega_m)\rho_{m,0}\kappa^2}{\rho_{m,0}\kappa^2-3H^2\mathrm{e}^{\frac{3(1+\omega_m)H}{(1+\alpha)}\left(\frac{H}{\beta}\right)^{\frac{1}{\alpha}}}}. \tag{53}$$

The above expression has been evaluated by recalling Eqs. (47) and (48). In the physical models, we have $\kappa^2\equiv 8\pi G=1.68\times10^{-9}$ m^3/kg/s^2, and $\rho_{m,0}=2.84\times10^{-27}$ kg/m^3. Therefore, the value $\kappa^2\rho_{m,0}\to 0$ s^{-2} so that Eq. (53) reduces to

$$\omega_T\to -1-\frac{2}{3}\frac{\alpha}{H}\left(\frac{\beta}{H}\right)^{\frac{1}{\alpha}}=\omega_{\rm eff},$$

which coincides with the effective equation of state (50). In order to investigate the exact role of the torsion fluid, it is convenient to study the behavior of the torsion equation of state near the singularity. It is clear from Eq. (53) that the torsion equation of state is too sensitive to the choices of the parameters α and β. Therefore, we will discuss each case individually in the following sections.

In Section 2, we presented a generic study of the different types of finite-time singularities by analyzing their phase portraits. In the following, we perform a complementary analysis of the cosmologies related to these singularity types through the effective and the torsion equations of state to find out the role of the torsion fluid and its behavior near these singularities. In fact, the cosmic accelerated expansion can be modeled using the cosmological constant in the simplest case, when this constant is introduced into Einstein's field equations as a matter source of so-called dark energy with a fixed equation of state $\omega=-1$. Although it fits with the Planck observations, it does not provide information about the nature of the dark energy. Other proposals have been introduced using a quintessence ($-1<\omega<-1/3$) or phantom ($\omega<-1$) scalar field, where crossing between these two regimes within the single canonical scalar field models is impossible [92]. This is contrary to the quintom models, where crossing the phantom divide line can be achieved. A comprehensive criticism of quintom bounce is given in the review in Ref. [93]. Usually, quintom models are realizable by introducing two scalar fields (quintessence + phantom) [94, 95], or adding extra degrees of freedom by including higher derivative terms into the action [96–98]. As we have shown, the $f(T)$ cosmology provides a dynamical system equivalent to the general relativistic model when using an exotic equation of state, e.g. quintessence, phantom or quintom. This equivalence can also be justified by studying the role of the torsion equation of state.

4.1 Type I singularity

Using Eqs. (50) and (53), we plot their evolutions as given in Fig. 7. As we have shown earlier in Section 2.1, there are two cases which can be discussed for models with singularities of Type I ($\alpha<-1$):

4.1.1 $f_0>0$ ($\beta<0$)

As we have discussed for this case using the phase portrait, Fig. 2(a), the universe begins with a finite-time

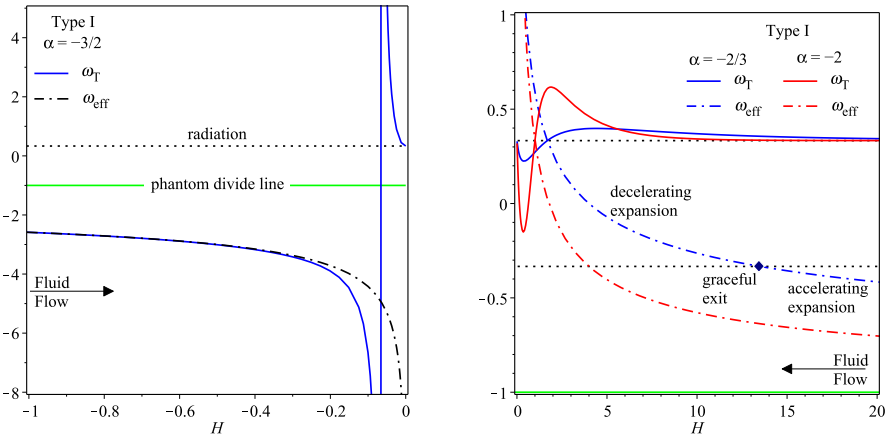

(a) $f_0>0$ ($\beta<0$) (b) $f_0<0$ ($\beta>0$)

Fig. 7. (color online) The evolution of the effective and the torsion equation of state parameters, Eqs. (50) and (53), in the vicinity of a finite-time singularity of Type I.

singularity of Type I in a contracting phase in a phantom regime, and evolves towards a future fixed point $H\to 0$ in an infinite time. Using Eqs. (50) and (53), we have, at the limit $H\to-\infty$, and the universe effectively follows the torsion fluid as $\omega_{\rm eff}=\omega_T\to-1$. At the limit $H\to 0$, the effective equation of state diverges as $\omega_{\rm eff}=Q_0\to-\infty$ but the universe needs an infinite time to approach that fate. Therefore, the universe will not feel this future singularity. On the other hand, the torsion fluid evolves towards $\omega_T\to-\infty$ similar to the effective fluid, but in a finite time. As seen in Fig. 7(a), the irregular behavior of torsion fluid is just before the Minkowskian fixed point, where the torsion equation of state parameter changes its sign from $-\infty$ to $+\infty$. This behavior usually results in sudden singularities. In other words, although the universe effectively will not feel the singularity at the fixed point, the torsion fluid feels it as a finite-time singularity of Type II. However, the torsion fluid crosses the phantom divide line through a singularity, then it evolves towards the matter equation of state, i.e. $\omega_T\to\omega_m$, as its final fate.

We note that the limits of Eqs. (50) and (53) are both regular at $H\to+\infty$, where $\omega_{\rm eff}=\omega_T\to-1$. Guided by the phase portraits of Fig. 2, we should ignore these limits. However, we record them in Table 2 in Section 5 just for completeness.

4.1.2 $f_0<0$ ($\beta>0$)

In these models, the universe begins with a finite-time singularity of Type I (big bang) similar to the standard cosmology. However, it experiences an early accelerated expansion phase, then enters a later decelerating phase. For more details, recall Section 2.1.2.

Case 1. In the subclass $-2<\alpha<-1$, the universe begins with a big bang singularity where the asymptotic behavior of the effective equation of state (50) can be obtained as $\omega_{\rm eff}\to-1$ as $H\to\infty$. As seen in Fig. 7(b), the universe effectively crosses $\omega_{\rm eff}=-1/3$ ending the early inflationary phase, and enters a late deceleration phase as $\omega_{\rm eff}>-1/3$. We note that the plots of Fig. 7(b) are just to visualize the qualitative behavior of the model. For physical models, however, one may consult Fig. 6(b) to use the correct values of the parameters α and β in order to end the inflation period at a suitable energy scale $10^7<H<10^9$ GeV. Then, the effective equation of state diverges, i.e. $\omega_{\rm eff}=Q_0\to+\infty$ as H drops to zero. That is, a fixed point and effective fluid takes an infinite time to reach that point. On the other hand, using Eq. (53), we find that the torsion fluid matches the matter fluid during cosmic time, $\omega_T\sim\omega_m$, with an oscillatory behavior at the limit $H\to 0$.

Case 2. In the subclass $\alpha\leqslant-2$, the evolution is very similar to case 1 above, as seen in Fig. 7(b). However, we find that the torsion equation of state has an asymptotic behavior $\omega_T\to-1$ at the limit $H\to-\infty$ instead of ω_m. This is shown in Table 2 in Section 5. However, the negative H region should be excluded as guided by the phase portraits in Fig. 2(b). So we note that the two cases of $\beta>0$, in general, are identical.

4.2 Type II singularity

Using Eqs. (50) and (53), we plot their evolutions as shown in Fig. 8. As in Section 2.2, we discuss two main categories of the models which have a Type II singularity ($0<\alpha<1$), $\beta<0$ and $\beta>0$. Recalling the phase portraits of Fig. 3, we note that the singularity is at $H_s=0$, where $\dot H$ diverges. This leads the effective pressure to diverge as well. Consequently, it will be common for all the following categories to have a divergent effective equation of state at that point, i.e. $\omega_{\rm eff}\to\pm\infty$ as $H\to 0$.

4.2.1 $f_0<0$ ($\beta<0$)

Case 1. In the subclass $\alpha=\frac{1}{n}$ (where ($n>1$ is an odd positive integer), we plot the evolution of both the effective equation of state and the torsion equation of

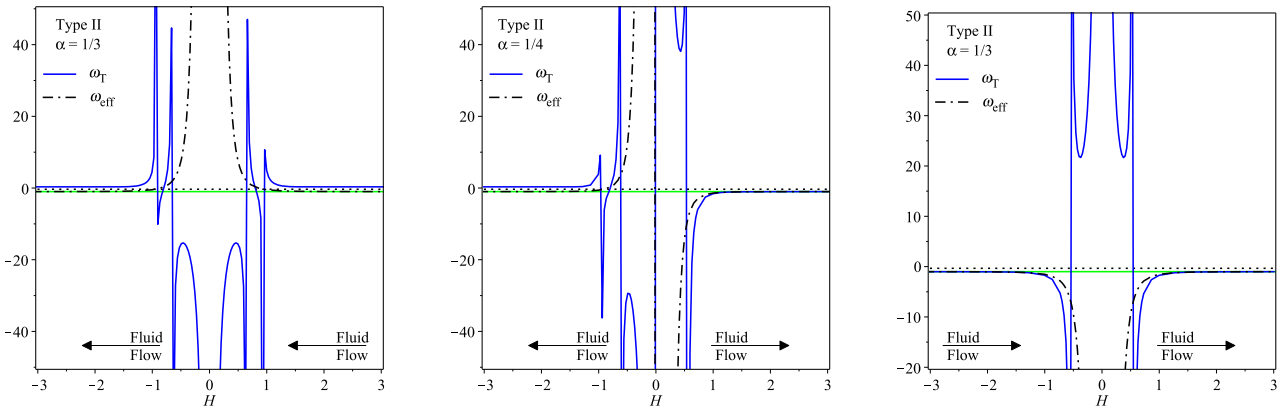

(a) $\alpha=\frac{1}{n}$, n = odd ($\beta<0$) (b) $\alpha=\frac{1}{n}$, n = even ($\beta<0$ or $\beta>0$) (c) $\alpha=\frac{1}{n}$, n = odd ($\beta>0$)

Fig. 8. (color online) The evolution of the effective and the torsion equation of state parameters, Eqs. (50) and (53), in the vicinity of a finite-time singularity of Type II.

state as shown in Fig. 8(a). The evolution goes in the direction of decreasing Hubble parameter. Since the singularity is not of a crashing type and the geodesics are complete, a transition from expansion to contraction is conceivable. This can be called a big brake model. These usually suffer from a singularity crossing paradox, where tachyon cosmological models [9] or anti-Chaplygin gas [4] play an essential role in making the singularity crossing physically possible. We note, for this model, that the torsion fluid asymptotically matches the matter component, i.e. $\omega_T \to \omega_m$. However, its equation of state feels the singularity earlier and becomes irregular. In the vicinity of the singularity $H \to 0^{\pm}$, from Eq. (53), we have

$$\lim_{H\to 0^{\pm}} \omega_T = Q_1 \to -\infty; \text{ since } \beta<0 \text{ and } 0<\alpha<1, \quad (54)$$

where $Q_1 \equiv Q_1(H) = \frac{2}{\rho_0 \kappa^2}\alpha H \left(\frac{\beta}{H}\right)^{1/\alpha}$. However, in the contraction phase the torsion fluid evolves towards the matter component.

Case 2. In the subclass $\alpha = \frac{1}{n}$ (where $(n>1$ is an even positive integer), we plot the evolution of both the effective equation of state and the torsion equation of state as shown in Fig. 8(b). The sudden singularity at $H=0$ acts as a repeller; the universe evolves with increasing Hubble parameter in the $H>0$ region and it evolves with decreasing Hubble parameter in the $H<0$ region. In this subclass, the effective fluid evolves in the vicinity of the singularity as

$$\lim_{H\to 0^{\pm}} \omega_{\text{eff}} = Q_0 \to \mp\infty,$$

while it asymptotically evolves towards the cosmological constant, i.e. $\omega_{\text{eff}} \to -1$ as $H \to \pm\infty$. In the right-hand region, the torsion evolves towards a cosmological constant, i.e. $\omega_T \to -1$ as $H \to +\infty$. In the left-hand region, it evolves towards the matter component, i.e. $\omega_T \to \omega_m$ as $H \to -\infty$. However, in the vicinity of the singularity $H=0$, the torsion equation of state alters its sign opposite to the effective fluid as

$$\lim_{H\to 0^{\pm}} \omega_T = Q_1 \to \pm\infty.$$

Case 3. In the subclass $\alpha = \frac{a}{b} \neq \frac{1}{n}$, where ($a$ and b are positive integers such that $a<b$), we find two patterns. The first is when $0<\alpha<1/2$; it follows case 2 and can be visualized in Fig. 8(a). The second is when $1/2<\alpha<1$; it follows case 1 and can be visualized in Fig. 8(b). For both cases, only the $H<0$ region is allowed for this subclass.

4.2.2 $f_0>0$ ($\beta>0$)

Case 1. In the subclass $\alpha = \frac{1}{n}$ (where $(n>1$ is an odd positive integer), we plot the evolution of both the effective equation of state and the torsion equation of state as shown in Fig. 8(c). This subclass can be used to describe a bouncing cosmology model, since crossing the singularity at $H=0$ from contraction ($H<0$) to expansion ($H>0$) is a valid scenario. In general, bouncing models suffer from two main problems: ghost instability and anisotropy growth. The first arises when the null energy condition has been broken. In $f(T)$ gravity, it has been shown that the null energy condition is violated effectively only, while the matter component is free from forming ghost degrees of freedom [23]. The second problem arises during the contraction phase before bounce, since the anisotropies grow faster than the background so that the universe ends up as a complete anisotropic universe and bouncing to expansion will not occur.

As shown in Fig. 8(c), the effective fluid acts asymptotically $H \to \pm\infty$ as a cosmological constant $\omega_{\text{eff}} \to -1$, then it runs deeply in the phantom regime near the singular bounce as

$$\lim_{H\to \pm} \omega_{\text{eff}} = Q_0 \to -\infty.$$

However, the torsion fluid in the vicinity of the bouncing (singular) point has a large equation of state,

$$\lim_{H\to 0^{\pm}} \omega_T = Q_1 \to +\infty,$$

which allows the torsion gravity background to dominate over the anisotropy during the contraction, avoiding the main remaining problem of bouncing models. Therefore, the model at hand can be considered as a healthy bouncing scenario, where the torsion gravity plays the main role to avoid the usual problems of bounce cosmological models.

Case 2. In the subclass $\alpha = \frac{1}{n}$ (where $(n>1$ is an even positive integer), the evolution is identical to that obtained in case 2 of Section 4.2.1, so the evolution can be realized from Fig. 8(b).

Case 3. In the subclass $\alpha = \frac{a}{b} \neq \frac{1}{n}$, where ($a$ and b are positive integers such that $a<b$), we find two patterns. The first is when $0<\alpha<1/2$. It follows case 2 and can be visualized in Fig. 8(c). The second is when $1/2<\alpha<1$, which follows case 1 and can be visualized in Fig. 8(b). For both, only the $H>0$ region is valid, and the $H<0$ region is not allowed for this subclass.

We note that the asymptotic behavior of both the effective and the torsion equations of state in the vicinity of the Type II finite-time singularity is summarized in Table 2 in Section 5.

4.3 Type III singularity

Using Eqs. (50) and (53), we plot their evolutions as given in Fig. 9. As in Section 2.2, we discuss two main categories of the models which have Type III singularities ($-1<\alpha<0$), $\beta<0$ and $\beta>0$.

4.3.1 $f_0<0$ ($\beta<0$)

Case 1. In the subclass $\alpha = -\frac{1}{n}$ (where $(n>1$ is an odd positive integer), we plot the evolution of both the effective and the torsion equations of state as shown in

Fig. 9(a). From Eqs. (50) and (53), we find that both equation of state parameters, asymptotically, evolve as $\omega_{\rm eff}=\omega_T=Q_0\to-\infty$ as $H\to\pm\infty$. However, as $H\to0$, the effective fluid evolves towards a cosmological constant, i.e $\omega_{\rm eff}\to-1$, while the torsion fluid evolves towards the matter component, i.e. $\omega_T\to\omega_m$. In other words, the universe evolves effectively in a phantom regime towards the cosmological constant, while the torsion fluid crosses the phantom divide line towards the matter component at that point. We note that the point $H=0$ is a fixed point so the fluids reaches the mentioned fate in an infinite time, while asymptotically there are finite-time singularities of Type III, and therefore, they reach their fate in a finite time. Also, the evolution in both regions, $H<0$ and $H>0$, occur in the phantom regime as $\omega_{\rm eff}<-1$. This is in agreement with the corresponding phase portraits of Fig. 4(a).

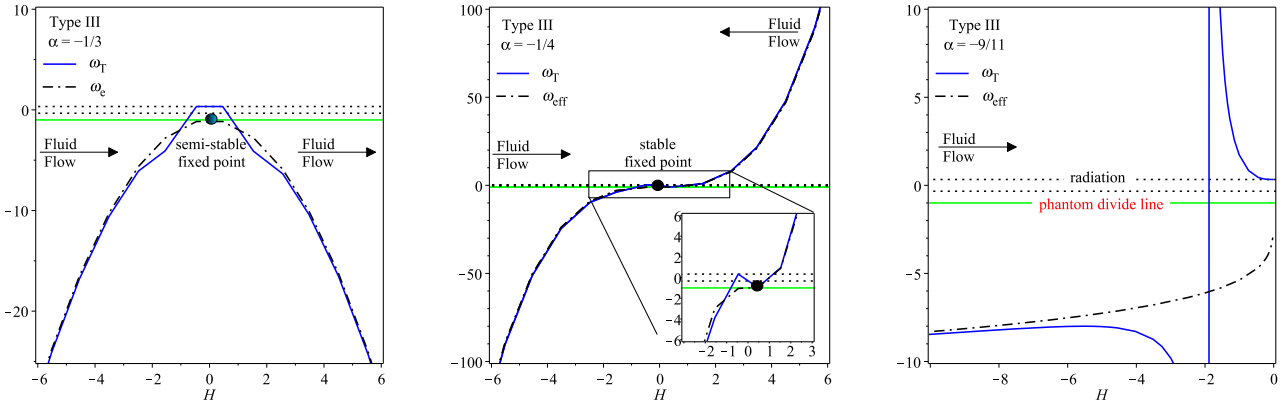

(a) $\alpha=-\frac{1}{n}$, n = odd ($\beta<0$) (b) $\alpha=-\frac{1}{n}$, n = even ($\beta<0$ or $\beta>0$) (c) $-1<\alpha=-\frac{a}{b}\neq-\frac{1}{n}<-1/2$ ($\beta<0$)

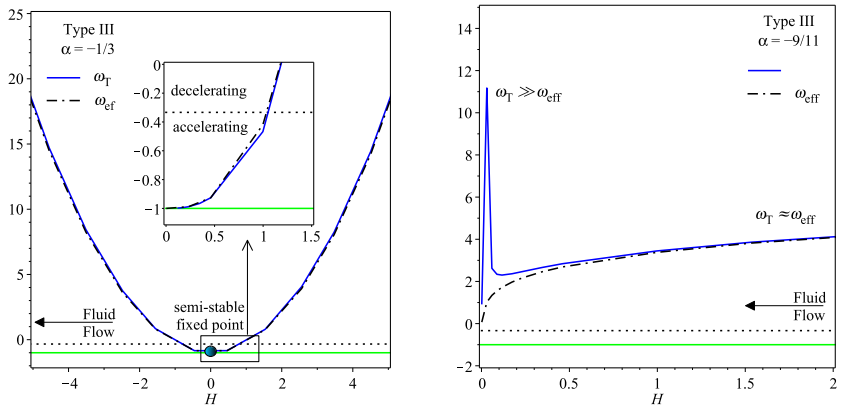

(d) $\alpha=-\frac{1}{n}$, n = odd ($\beta>0$) (e) $-1<\alpha=-\frac{a}{b}\neq-\frac{1}{n}<-1/2$ ($\beta>0$)

Fig. 9. (color online) The evolution of the effective and the torsion equation of state parameters, Eqs. (50) and (53), in the vicinity of a finite-time singularity of Type III.

Case 2. In the subclass $\alpha=-\frac{1}{n}$ (where ($n>1$ is an even positive integer), we plot the evolution of both the effective and the torsion equations of state as shown in Fig. 9(b). From Eqs. (50) and (53), noting that n is even and $\beta<0$ in the case at hand, the sign of the asymptotic behavior will be sensitive only to the sign of the Hubble parameter. Thus, we write

$$\lim_{H\to\pm\infty}\omega_{\rm eff}=\lim_{H\to\pm\infty}\omega_T=Q_0\to\pm\infty.$$

However, at the limit $H\to0$, both fluids evolve towards the cosmological constant, i.e. $\omega_{\rm eff}=\omega_T\to-1$. As is clear from Fig. 9(b), in the $H<0$ region the universe evolves effectively in the phantom regime towards a cosmological constant. However, in the $H>0$ region the universe evolves effectively in a non phantom regime towards the cosmological constant at the Minkowski fixed point universe, so it realizes a late transition to accelerating expansion universe as it crosses from $\omega_{\rm eff}>-1/3$ to $-1<\omega_{\rm eff}<-1/3$. Although we can choose suitable values of α and β, as shown in Section 2.5, to realize the late transition at redshift $z_{de}\sim0.7$ as required by the ΛCDM model, the universe evolves towards a Minkowski rather than a de Sitter universe. This is not usual when dark energy is interpreted as a cosmological constant.

Case 3. In the subclass $\alpha=-\frac{a}{b}\neq-\frac{1}{n}$, where ($a$ and b are positive integers such that $a<b$), we find two patterns. The first is when $-1/2<\alpha<0$, it follows case 2 and can be visualized in Fig. 9(a), but only the $H<0$ region, as the $H>0$ region is not allowed for this subclass. The second is when $-1<\alpha<-1/2$, where the evolution at the limits $H\to0$, $\pm\infty$ follows case 1 as given in Table 2 in Section 5. However, we plot the instantaneous evolution of both the effective equation of state and the torsion equation of state as shown in Fig. 9(c), where the $H<0$ region is the only valid scenario.

4.3.2 $f_0>0$ ($\beta>0$)

Case 1. In the subclass $\alpha=-\frac{1}{n}$ (where ($n>1$ is an odd positive integer), we plot the evolution of both the effective and the torsion equations of state as appear in Fig. 9(d). From Eqs. (50) and (53), we find that both equation of state parameters, asymptotically, evolve as $\omega_{\rm eff}=\omega_T=Q_0\to+\infty$ as $H\to\pm\infty$. This is opposite to the similar case of Section 4.3.1 as we examine $\beta>0$ in this section. However, as $H\to0$, both parameters evolve towards the cosmological constant, i.e $\omega_{\rm eff}=\omega_T\to-1$. Thus, the universe evolves effectively in a non phantom regime towards the cosmological constant, where a late transition from acceleration to deceleration is valid. This is in agreement with the corresponding phase portraits of Fig. 4(a).

Case 2. In the subclass $\alpha=-\frac{1}{n}$ (where ($n>1$ is an even positive integer), the evolution is identical to that has been obtained in case 2 of Section 4.3.1. So the evolution can be realized from Fig. 9(b).

Case 3. In the subclass $\alpha=-\frac{a}{b}\neq-\frac{1}{n}$, where ($a$ and b are positive integers such that $a<b$), we find two patterns. The first is when $-1/2<\alpha<0$. It follows case 2 and can be visualized in Fig. 9(d), but only for the $H>0$ region, as the $H<0$ region is not allowed for this subclass. The second is when $-1<\alpha<-1/2$. We plot the evolution of both the effective equation of state and the torsion equation of state as shown in Fig. 9(e). From Eqs. (50) and (53), we find that both equation of state parameters, asymptotically, evolve as

$$\lim_{H\to\pm\infty}\omega_{\rm eff}=\lim_{H\to\pm\infty}\omega_T=Q_0\to\pm\infty,$$

with the $H<0$ region not allowed for this class. At the limit $H\to0$, both parameters evolve towards the cosmological constant. However, the torsion fluid parameter can be irregular in the vicinity of that point.

All three cases above where $\beta>0$, in addition to case 2 with $\beta<0$, can perform a late deceleration to acceleration transition. For possible suitable choices of the parameters α and β, recall Section 2.5, in particular Fig. 6(c).

4.4 Type IV singularity

Using Eqs. (50) and (53), we plot their evolutions as given in Fig. 10. As we have shown earlier in Section 2.4, two cases can be discussed for the models which have a Type IV ($\alpha>1$) singularity.

4.4.1 $f_0>0$ ($\beta<0$)

As discussed for this case using the phase portrait, Fig. 5, the universe begins with a finite-time singularity

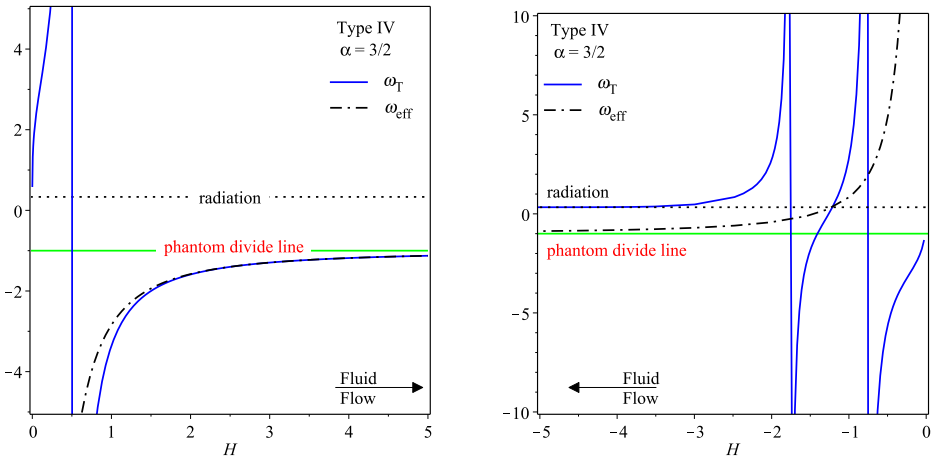

(a) $f_0>0$ ($\beta<0$) (b) $f_0<0$ ($\beta>0$)

Fig. 10. (color online) The evolution of the effective and the torsion equation of state parameters, Eqs. (50) and (53), in the vicinity of a finite-time singularity of Type IV.

Table 2. The evolution of the effective/torsion equations of state (50) and (53) near $H\to 0,\ \pm\infty$, corresponding to different choices of α and β parameters. We take $n>1$ ($m>1$) as a positive odd (even) integer, and $a<b$ where a and b are positive integers.

	parameters			$\omega_{\rm eff}$			ω_T		
singularity	f_0	β	α	$H\to 0^{\pm}$	$H\to\infty$	$H\to-\infty$	$H\to 0^{\pm}$	$H\to\infty$	$H\to-\infty$
Type I	>0	<0	<-1	$Q_0\to-\infty$	-1	-1	ω_m	-1	-1
	<0	>0	$\in(-2,-1)$	$Q_0\to+\infty$	-1	-1	ω_m	ω_m	ω_m
			$\leqslant -2$	$Q_0\to+\infty$	-1	-1	ω_m	ω_m	-1
Type II	<0	<0	$\frac{1}{n}$ or $\frac{1}{2}<\frac{a}{b}\neq\frac{1}{n}<1$	$Q_0\to+\infty$	-1	-1	$Q_1\to-\infty$	ω_m	ω_m
			$\frac{1}{m}$ or $0<\frac{a}{b}\neq\frac{1}{m}<\frac{1}{2}$	$Q_0\to\mp\infty$	-1	-1	$Q_1\to\pm\infty$	-1	ω_m
	>0	>0	$\frac{1}{n}$ or $\frac{1}{2}<\frac{a}{b}\neq\frac{1}{n}<1$	$Q_0\to-\infty$	-1	-1	$Q_1\to+\infty$	-1	-1
			$\frac{1}{m}$ or $0<\frac{a}{b}\neq\frac{1}{m}<\frac{1}{2}$	$Q_0\to\mp\infty$	-1	-1	$Q_1\to\pm\infty$	-1	ω_m
Type III	<0	<0	$\frac{-1}{n}$ or $-1<\frac{-a}{b}\neq\frac{-1}{n}<\frac{-1}{2}$	-1	$Q_0\to-\infty$	$Q_0\to-\infty$	ω_m	$Q_0\to-\infty$	$Q_0\to-\infty$
			$\frac{-1}{m}$ or $\frac{-1}{2}<\frac{-a}{b}\neq\frac{-1}{m}<0$	-1	$Q_0\to+\infty$	$Q_0\to-\infty$	-1	$Q_0\to+\infty$	$Q_0\to-\infty$
	>0	>0	$\frac{-1}{n}$ or $-1<\frac{-a}{b}\neq\frac{-1}{n}<\frac{-1}{2}$	-1	$Q_0\to+\infty$	$Q_0\to+\infty$	-1	$Q_0\to+\infty$	$Q_0\to+\infty$
			$\frac{-1}{m}$ or $\frac{-1}{2}<\frac{-a}{b}\neq\frac{-1}{m}<0$	-1	$Q_0\to+\infty$	$Q_0\to-\infty$	-1	$Q_0\to+\infty$	$Q_0\to-\infty$
Type IV	>0	<0	>1	$Q_0\to-\infty$	-1	-1	ω_m	-1	-1
	<0	>0	$\in(1,2)$	$Q_0\to+\infty$	-1	-1	ω_m	ω_m	ω_m
			$\geqslant 2$	$Q_0\to+\infty$	-1	-1	ω_m	-1	ω_m

Note: The quantities Q_0 and Q_1 above are as given in Eqs. (51) and (54), respectively.

of Type IV in Minkowski space, which is a fixed point as well. Therefore, the corresponding effective equation of state parameter has an infinite value at the Minkowiskian point. From Eq. (50), we have

$$\lim_{H\to 0^+}\omega_{\rm eff}=Q_0=-\infty.$$

However, the torsion fluid at the same limit begins with an equation of state parameter equivalent to the matter component, i.e. $\omega_T\to\omega_m$ as $H\to 0$. Then the effective fluid evolves, in the phantom regime, smoothly towards the cosmological constant, $\omega_{\rm eff}\to-1$, in increasing H direction. On the other hand, the torsion equation of state parameter matches the effective fluid asymptotically as $H\to+\infty$. It is irregular in the vicinity of the initial singularity. Since ω_T changes its sign near the singularity, it feels the singularity of Type IV as if it is a sudden singularity, see Fig. 10(a). Recalling Eq. (9) and the related discussion, we find that the effective fluid will not be singular at $H\to\infty$, and consequently the torsion fluid as $\omega_{\rm eff}\sim\omega_T$ at that limit.

4.4.2 $f_0<0$ ($\beta>0$)

Alternatively, in these models, the universe begins effectively with $\omega_{\rm eff}\to+\infty$ in a singular Minkowskian universe of Type IV. However, the torsion equation of state parameter initially begins with a value equivalent to the matter component, see Fig. 10(a). Only the $H<0$ region is allowed in this scenario, so the universe contracts with a deceleration after the Minkowskian universe as $\omega_{\rm eff}>-1/3$, then it crosses the quintessence limit towards the cosmological constant asymptotically as $H\to-\infty$. The torsion fluid matches the matter component at that limit.

We note that the torsion fluid in the two subclasses $-2<\alpha<-1$ and $\alpha\leqslant-2$ has different limits at $H\to+\infty$. In the first subclass, the torsion fluid evolves asymptotically towards the matter component, while it evolves towards the cosmological constant in the second. However, the positive H region should be excluded for $\beta>0$, as guided by the phase portraits in Fig. 5. So we note that the two cases of $\beta>0$, in general, are identical.

Finally, as clear from the discussions throughout this work, investigating the asymptotic solutions and the fixed points is essential to understand one-dimensional autonomous dynamical systems. We summarize all the limits of the effective and the torsion equation of state parameters at $H\to 0,\ \pm\infty$ as given in Table 2 in Section 5.

5 Concluding remarks

For a modified gravity theory and by assuming the effective fluid has a linear equation of state, we have shown that the Friedmann equations can represent a one-dimensional autonomous system, if the first derivative of the Hubble parameter is written as a function of the Hubble parameter only. This allows us to interpret the Friedmann system as a vector field on a line, introducing one of the basic techniques of dynamics. Consequently, we draw the $(H-\dot{H})$, phase space allowing a clear geometrical representation of the dynamical system by identifying its fixed points and asymptotic behavior.

In this paper we have investigated phase portraits of the different types of finite-time singularities. We adopted a scale factor containing two model parameters α and β, which can realize the finite-time singularity types. General analysis of the phase portraits has shown that:

(1) For a singularity of Type I ($\alpha<-1$), the model realizes an early accelerating expansion (inflation) with possible transition to a later decelerated expansion for some suitable values $\beta>0$. We plot the viable values of α and β which allow this transition to occur at a cosmic energy scale 10^9 to 10^7 GeV, when inflation is assumed to be during 10^{-34} and 10^{-31} s. This provides suitable conditions for a graceful exit inflation model.

(2) For a singularity of Type II ($0<\alpha<1$), when α is chosen such that $\alpha=\dfrac{1}{n}$ and n is a positive integer, the universe evolves effectively in a phantom regime. The universe contracts before the singularity, while it expands after it. This may give a singular bounce with a finite-time singularity at the bouncing time. However, junction conditions could be used to overcome the singularity by welding the contraction an the expansion phases around the singularity point. This point needs further investigation.

(3) For a singularity of Type III ($-1<\alpha<0$), the model realizes a late transition from decelerating to accelerating expansion. We plot the viable values of α and β which allow this transition to occur at redshift $z_{de}=0.72\pm0.05$ (0.84 ± 0.03), i.e. $H_{de}=101.8$ (117.82) km/s/Mpc. Although the model realizes the transition to the late accelerating expansion phase, it evolves towards a Minkowski and not a de Sitter fate as expected by the ΛCDM models. This is unusual when dark energy is assumed to be a cosmological constant.

(4) For a singularity of Type IV ($\alpha>1$), the singular point is also a repeller fixed point, which provides an unstable de Sitter universe. In this case, we expect unusual behavior by having a fixed point that can be reached at a finite time. The phase portrait analysis show that the Type IV singularities can be used for crossing between phantom and non phantom cosmologies safely as the geodesics in this model are completed.

We also shown that torsion based gravity is compatible with the phase portrait analysis. This is because the teleparallel torsion T is a function of the Hubble parameter H only and it contains no higher derivatives of H. Consequently, it allows the modified Friedmann system to be written as a one-dimensional autonomous system. Among several versions of the generalized teleparallel gravity, we investigated the $f(T)$ gravity theories.

We reconstructed the $f(T)$ function which generates the proposed phase portraits. This allows us to perform a complementary investigation of the singularity types through the torsion equation of state. In addition, we note that since some cases of the singularities are in fact a Minkowskian space rather a de Sitter one, an investigation of the torsion role in the vicinity of different singularity types on the perturbation level will be needed. For perturbation analysis in $f(T)$ see Refs. [20, 23, 99, 100]. In fact the singular phases can be shifted from Minkowski to de Sitter as needed by modifying the phase portrait (8) by adding a constant H_{ds}. As we have shown, the dynamics of one-dimensional autonomous systems is dominated by the stability of the fixed points and the asymptotic behavior. We summarize the results obtained in Table 2.

The authors would like to thank Prof. A. Awad for several discussions.

References

1 Shin'ichi Nojiri and Sergei D. Odintsov, Phys. Lett. B, **595**: 1–8 (2004), arXiv:hep-th/0405078 [hep-th]

2 Petr Tretyakov, Aleksey Toporensky, Yuri Shtanov, and Varun Sahni, Class. Quant. Grav., **23**: 3259–3274 (2006), arXiv:gr-qc/0510104 [gr-qc]

3 John D. Barrow, Antonio B. Batista, Julio C. Fabris, Mahouton J. S. Houndjo, and Giuseppe Dito, Phys. Rev. D, **84**: 123518 (2011), arXiv:1110.1321 [gr-qc]

4 Zoltan Keresztes, Laszlo A. Gergely, and Alexander Yu. Kamenshchik, Phys. Rev. D, **86**: 063522 (2012), arXiv:1204.1199 [gr-qc]

5 John D. Barrow and S. Cotsakis, Phys. Rev. D, **88**: 067301 (2013), arXiv:1307.5005 [gr-qc]

6 A. Yu. Kamenshchik, E. O. Pozdeeva, Sergey Yu. Vernov, A. Tronconi, and G. Venturi, Phys. Rev. D, **94**: 063510 (2016), arXiv:1602.07192 [gr-qc]

7 A. Awad and G. Nashed, J. Cosm. Astropart. Phys., **2**: 046 (2017), arXiv:1701.06899 [gr-qc]

8 Mariusz P. Dabrowski, Tomasz Denkiewicz, and Martin A. Hendry, Phys. Rev. D, **75**: 123524 (2007), arXiv:0704.1383 [astro-ph]

9 Z. Keresztes, L. A. Gergely, V. Gorini, U. Moschella, and A. Yu. Kamenshchik, Phys. Rev. D, **79**: 083504 (2009), arXiv:0901.2292 [gr-qc]

10 K. Kleidis and V. K. Oikonomou, Astrophys. Space Sci., **361**: 326 (2016), arXiv:1609.00848 [gr-qc]
11 Jerome Martin and Robert H. Brandenberger, Phys. Rev. , 123501 (2001), arXiv:hep-th/0005209 [hep-th]
12 Robert H. Brandenberger and Jerome Martin, Class. Quant. Grav., **30**: 113001 (2013), arXiv:1211.6753 [astro-ph.CO]
13 David Wands, Phys. Rev. , 023507 (1999), arXiv:gr-qc/9809062 [gr-qc]
14 Fabio Finelli and Robert Brandenberger, Phys. Rev. , 103522 (2002), arXiv:hep-th/0112249 [hep-th]
15 Tirthabir Biswas, Riley Mayes, and Colleen Lattyak, Phys. Rev. , 063505 (2016), arXiv:1502.05875 [gr-qc]
16 M. Novello and S. E. Perez Bergliaffa, Phys. Rept., **463**: 127–213 (2008), arXiv:0802.1634 [astro-ph]
17 Yi-Fu Cai, Sci. China Phys. Mech. Astron., **57**: 1414–1430 (2014), arXiv:1405.1369 [hep-th]
18 D. Battefeld and Patrick Peter, Phys. Rept., **571**: 1–66 (2015), arXiv:1406.2790 [astro-ph.CO]
19 Robert Brandenberger and Patrick Peter, Found. Phys., **47**: 797–850 (2017), arXiv:1603.05834 [hep-th]
20 Y.-F. Cai, S.-H. Chen, J. B. Dent, S. Dutta, and E. N. Saridakis, Classical and Quantum Gravity, **28**: 215011 (2011), arXiv:1104.4349 [astro-ph]
21 Jaume Amorós, Jaume de Haro, and Sergei D. Odintsov, Phys. Rev. D, **87**: 104037 (2013), arXiv:1305.2344 [gr-qc]
22 S. D. Odintsov and V. K. Oikonomou, Int. J. Mod. Phys. , 1750085 (2017), arXiv:1512.04787 [gr-qc]
23 Kazuharu Bamba, G. G. L. Nashed, W. El Hanafy, and S.K. Ibraheem, Phys. Rev. D, **94**: (2016), 10.1103/PhysRevD.94.083513, arXiv:1604.07604 [gr-qc]
24 W. El Hanafy and G. G. L. Nashed, Int. J. Mod. Phys. , 1750154 (2017), arXiv:1707.01802 [gr-qc]
25 Shin'ichi Nojiri, Sergei D. Odintsov, and Shinji Tsujikawa, Phys. Rev. D, **71**: 063004 (2005), arXiv:hep-th/0501025 [hep-th]
26 Shin'ichi Nojiri and Sergei D. Odintsov, Phys. Rev. D, **78**: 046006 (2008), arXiv:0804.3519 [hep-th]
27 John D. Barrow, Class. Quant. Grav., **21**: L79–L82 (2004), arXiv:gr-qc/0403084 [gr-qc]
28 John D. Barrow, Class. Quant. Grav., **21**: 5619–5622 (2004), arXiv:gr-qc/0409062 [gr-qc]
29 S. D. Odintsov and V. K. Oikonomou, Phys. Rev. D, **92**: 124024 (2015), arXiv:1510.04333 [gr-qc]
30 S. D. Odintsov and V. K. Oikonomou, Phys. Rev. D, **92**: 024058 (2015), arXiv:1507.05273 [gr-qc]
31 I. Brevik, V. V. Obukhov, and A. V. Timoshkin, Mod. Phys. Lett. A, **31**: 1650105 (2016), arXiv:1604.04748 [gr-qc]
32 A. Awad, Phys. Rev. D, **87**: 103001 (2013), [Erratum: Phys. Rev.D87,no.10,109902(2013)], arXiv:1303.2014 [gr-qc]
33 A. Awad, W. El Hanafy, G. G. L. Nashed, and E. N. Saridakis, (2017), arXiv:1710.10194
34 Steven H. Strogatz, *Nonlinear Dynamics And Chaos: With Applications To Physics, Biology, Chemistry And Engineering*, Studies in Nonlinearity, Vol. 1 (1994)
35 S. D. Odintsov and V. K. Oikonomou, Phys. Rev. D, **92**: 024016 (2015), arXiv:1504.06866 [gr-qc]
36 Omer Farooq, Foram Ranjeet Madiyar, Sara Crandall, and Bharat Ratra, (2016), arXiv:1607.03537 [astro-ph.CO]
37 S. Nojiri, S. D. Odintsov, and V. K. Oikonomou, Phys. Lett. B, **747**: 310–320 (2015), arXiv:1506.03307 [gr-qc]
38 J. W. Maluf, Ann. Phys. (Berlin), **525**: 339–357 (2013), arXiv:1303.3897 [gr-qc]
39 G. Kofinas and E.N. Saridakis, Phys. Rev. D, **90**: 084044 (2014), arXiv:1404.2249 [gr-qc]
40 Salvatore Capozziello, Mariafelicia De Laurentis, and Konstantinos F. Dialektopoulos, Eur. Phys. J. C, **76**, 629 (2016), arXiv:1609.09289 [gr-qc]
41 Martin Krššák and J. G. Pereira, Eur. Phys. J. C, **75**: 519 (2015), arXiv:1504.07683 [gr-qc]
42 M. Krššák and E. N. Saridakis, Classical and Quantum Gravity, **33**: 115009 (2016), arXiv:1510.08432 [gr-qc]
43 F. I. Mikhail and M. I. Wanas, Proc. Roy. Soc. London Ser. A,, **356**: 471–481 (1977)
44 F. I. Mikhail and M. I. Wanas, Int. J. Theoret. Phys., **20**: 671–680 (1981)
45 M. I. Wanas, Int. J. Theoret. Phys., **24, 6**: 639–651 (1985)
46 M. I. Wanas, Astrophys. Space Sci., **127**: 21–25 (1986)
47 M. I. Wanas, Astrophys. Space Sci., **258**: 237–248 (1998), arXiv:9904019 [gr-qc]
48 F. I. Mikhail, M. I. Wanas, and A. M. Eid, Astrophys. Space Sci., **228**: 221–237 (1995)
49 M. I. Wanas and M. E. Kahil, Gen. Rel. Grav., **31**: 1921 (1999), arXiv:gr-qc/9912007 [gr-qc]
50 Nabil L. Youssef and Amr M. Sid-Ahmed, Rep. Math. Phys,, **60**: 39–53 (2007), arXiv:0604111 [gr-qc]
51 Nabil L. Youssef and Amr M. Sid-Ahmed, Int. J. Geom. Meth. Mod. Phys., **5**: 1109–1135 (2008), arXiv:0805.1336 [math.DG]
52 Nabil L. Youssef and Waleed A. Elsayed, Rep. Math. Phys., **72**: 1–23 (2013), arXiv:1209.1379 [gr-qc]
53 M. I. Wanas, Turkish J. Phys., **24**: 473–488 (2000), arXiv:0010099 [gr-qc]
54 M. I. Wanas, Stud. Cercet. Stiin. Ser. Mat., **10**: 297–309 (2001), arXiv:0209050 [gr-qc]
55 M. I. Wanas, M. Melek, and M. E. Kahil, Gravit. & Cosmol., **6**: 319–322 (2000), arXiv:9812085 [gr-qc]
56 M. I. Wanas, M. Melek, and M. E. Kahil, in *Galaxies and their constituents at the highest angular resolutions*, IAU Symposium, Vol. 205: edited by R. T. Schilizzi (2001, p. 396) arXiv:0306086 [gr-qc]
57 M. I. Wanas, Int. J. Geom. Meth. Mod. Phys., **4**: 373–388 (2007), arXiv:0703036 [gr-qc]
58 M. I. Wanas, Adv. High Energy Phys., **2012**: Article ID 752613, 10 pages (2012)
59 M. I. Wanas and S. A. Ammar, Mod. Phys. Lett. A, **25**, 1705–1721 (2010), arXiv:0505092 [gr-qc]
60 M.I. Wanas, N.L. Youssef, W. El Hanafy, and S.N. Osman, Adv. Math. Phys., **2016** (2016), 10.1155/2016/1037849 arXiv:1611.06075 [gr-qc]
61 M. I. Wanas, Nabil L. Youssef, and W. El Hanafy, Grav. Cosmol., **23**: 105–118 (2017), arXiv:1404.2485 [gr-qc]
62 B. Li, T. P. Sotiriou, and J. D. Barrow, Phys. Rev. D, **83**: 064035 (2011), arXiv:1010.1041 [gr-qc]
63 T. P. Sotiriou, B. Li, and J. D. Barrow, Phys. Rev. D, **83**: 104030 (2011), arXiv:1012.4039 [gr-qc]
64 R. Ferraro and F. Fiorini, Phys. Rev. D, **91**: 064019 (2015), arXiv:1412.3424 [gr-qc]
65 G. G. L. Nashed, Chin. Phys., 020401 (2010), arXiv:0910.5124 [gr-qc]
66 G. R. Bengochea and R. Ferraro, Phys. Rev. D, **79**: 124019 (2009), arXiv:0812.1205 [astro-ph]
67 E. V. Linder, Phys. Rev. D, **81**: 127301 (2010), arXiv:1005.3039 [astro-ph]
68 S. Capozziello, V. F. Cardone, H. Farajollahi, and A. Ravanpak, Phys. Rev. D, **84**: 043527 (2011), arXiv:1108.2789 [astro-ph]
69 Salvatore Capozziello, Orlando Luongo, and Emmanuel N. Saridakis, Phys. Rev. D, **91**: 124037 (2015), arXiv:1503.02832 [gr-qc]
70 K. Bamba and C.-Q. Geng, J. Cosmol. Astropart. Phys., **11**: 008 (2011), arXiv:1109.1694 [gr-qc]
71 H. Mohseni Sadjadi, Physics Letters B, **718**: 270–275 (2012), arXiv:1210.0937 [gr-qc]
72 K. Bamba, R. Myrzakulov, S. Nojiri, and S. D. Odintsov, Phys. Rev. D, **85**: 104036 (2012), arXiv:1202.4057 [gr-qc]
73 K. Bamba, S. Capozziello, M. De Laurentis, S. Nojiri, and

D. Sáez-Gómez, Phys. Lett. B, **727**: 194–198 (2013), arXiv:1309.2698 [gr-qc]
74 K. Bamba, C.-Q. Geng, C.-C. Lee, and L.-W. Luo, J. Cosmol. Astropart. Phys. **1**: 021 (2011), arXiv:1011.0508 [astro-ph]
75 G .G. L. Nashed and W. El Hanafy, Eur. Phys. J. C, **74**: (2014), 10.1140/epjc/s10052-014-3099-5 arXiv:1403.0913 [gr-qc]
76 G. G. L. Nashed, Gen. Relativ. Gravit., **47**: 75 (2015), arXiv:1506.08695 [gr-qc]
77 W. El Hanafy and G. G. L. Nashed, Eur. Phys. J. C, **75** (2015), 10.1140/epjc/s10052-015-3501-y arXiv:1409.7199 [hep-th]
78 W. El Hanafy and G. G. L. Nashed, Astrophys. Space Sci., **361** (2016), 10.1007/s10509-016-2853-6 arXiv:1510.02337 [gr-qc]
79 W. El Hanafy and G. G. L. Nashed, Astrophys. Space Sci., **361** (2016), 10.1007/s10509-016-2786-0 arXiv:1410.2467 [hep-th]
80 Lorenzo Iorio, Ninfa Radicella, and Matteo Luca Ruggiero, J. Cosmol. Astropart. Phys., **1508**: 021 (2015), arXiv:1505.06996 [gr-qc]
81 W. El Hanafy and G. G. L. Nashed, Astrophys. Space Sci., **361** (2016), 10.1007/s10509-016-2662-y arXiv:1507.07377 [gr-qc]
82 Andrew DeBenedictis and Sasa Ilijic, Phys. Rev. D, **94**: 124025 (2016), arXiv:1609.07465 [gr-qc]
83 Gabriel Farrugia, Jackson Levi Said, and Matteo Luca Ruggiero, Phys. Rev. D, **93**: 104034 (2016), arXiv:1605.07614 [gr-qc]
84 Ednaldo L. B. Junior, Manuel E. Rodrigues, and Mahouton J. S. Houndjo, J. Cosmol. Astropart. Phys. **1510**: 060 (2015), arXiv:1503.07857 [gr-qc]
85 Salvatore Capozziello, P. A. Gonzalez, Emmanuel N. Saridakis, and Yerko Vasquez, JHEP, **02**: 039 (2013), arXiv:1210.1098 [hep-th]
86 G. G. L Nashed and W. El Hanafy, Eur. Phys. J. C, **77**: 90 (2017), arXiv:1612.05106 [gr-qc]
87 G. G. L. Nashed, Chaos Solitons Fractals, **15**: 841 (2003), arXiv:gr-qc/0301008 [gr-qc]
88 G. G. L. Nashed, Phys. Rev. , 104034 (2013), arXiv:1311.3131 [gr-qc]
89 G. G. L. Nashed, Gen. Rel. Grav., **45**: 1887–1899 (2013), arXiv:1502.05219 [gr-qc]
90 G. G. L. Nashed, Chinese Physics Letters, **29**: 050402 (2012), arXiv:1111.0003 [physics.gen-ph]
91 Yi-Fu Cai, Salvatore Capozziello, Mariafelicia De Laurentis, and Emmanuel N. Saridakis, Rept. Prog. Phys., **79**: 106901 (2016), arXiv:1511.07586 [gr-qc]
92 Jun-Qing Xia, Yi-Fu Cai, Tao-Tao Qiu, Gong-Bo Zhao, and Xinmin Zhang, Int. J. Mod. Phys. , 1229–1243 (2008), arXiv:astro-ph/0703202 [astro-ph]
93 Yi-Fu Cai, Emmanuel N. Saridakis, Mohammad R. Setare, and Jun-Qing Xia, Phys. Rept., **493**: 1–60 (2010), arXiv:0909.2776 [hep-th]
94 Bo Feng, Xiu-Lian Wang, and Xin-Min Zhang, Phys. Lett. , 35–41 (2005), arXiv:astro-ph/0404224 [astro-ph]
95 Zong-Kuan Guo, Yun-Song Piao, Xin-Min Zhang, and Yuan-Zhong Zhang, Phys. Lett. , 177–182 (2005), arXiv:astro-ph/0410654 [astro-ph]
96 Irina Ya. Aref'eva, A. S. Koshelev, and S. Yu. Vernov, Phys. Rev. , 064017 (2005), arXiv:astro-ph/0507067 [astro-ph]
97 Ming-zhe Li, Bo Feng, and Xin-min Zhang, JCAP, **0512**: 002 (2005), arXiv:hep-ph/0503268 [hep-ph]
98 I. Ya. Aref'eva and A. S. Koshelev, JHEP, **02**: 041 (2007), arXiv:hep-th/0605085 [hep-th]
99 S.-H. Chen, J. B. Dent, S. Dutta, and E. N. Saridakis, Phys. Rev. D, **83**: 023508 (2011), arXiv:1008.1250 [astro-ph]
100 K. Rezazadeh, A. Abdolmaleki, and K. Karami, J. High Energy Phys., **01**: 131 (2016), arXiv:1509.08769 [gr-qc]